OXFORD

Human Molecular Genetics, 2017, Vol. 26, No. 14 2747–2767

doi: 10.1093/hmg/ddx161
Advance Access Publication Date: 26 April 2017
Original Article

ORIGINAL ARTICLE

GTP binding regulates cellular localization of Parkinson's disease-associated LRRK2

Marian Blanca Ramírez[1], Antonio Jesús Lara Ordóñez[1], Elena Fdez[1], Jesús Madero-Pérez[1], Adriano Gonnelli[2], Matthieu Drouyer[3,4], Marie-Christine Chartier-Harlin[3,4], Jean-Marc Taymans[3,4], Luigi Bubacco[2] Elisa Greggio[2] and Sabine Hilfiker[1,*]

[1]Institute of Parasitology and Biomedicine 'López-Neyra', Consejo Superior de Investigaciones Científicas (CSIC), 18016 Granada, Spain, [2]Department of Biology, University of Padova, Padova 35121, Italy, [3]Univ. Lille, Inserm, CHU Lille, UMR-S 1172 - JPArc - Centre de Recherche Jean-Pierre AUBERT Neurosciences et Cancer, F-59000 Lille, France and [4]Inserm, UMR-S 1172 Early Stages of Parkinson's Disease Team, F-59000 Lille, France

*To whom correspondence should be addressed. Tel: +34 958 18 16 54; Fax: +34 958 18 16 32; Email: sabine.hilfiker@ipb.csic.es

Abstract

Mutations in leucine-rich repeat kinase 2 (LRRK2) comprise the most common cause of familial Parkinson's disease (PD), and sequence variants modify risk for sporadic PD. Previous studies indicate that LRRK2 interacts with microtubules (MTs) and alters MT-mediated vesicular transport processes. However, the molecular determinants within LRRK2 required for such interactions have remained unknown. Here, we report that most pathogenic LRRK2 mutants cause relocalization of LRRK2 to filamentous structures which colocalize with a subset of MTs, and an identical relocalization is seen upon pharmacological LRRK2 kinase inhibition. The pronounced colocalization with MTs does not correlate with alterations in LRRK2 kinase activity, but rather with increased GTP binding. Synthetic mutations which impair GTP binding, as well as LRRK2 GTP-binding inhibitors profoundly interfere with the abnormal localization of both pathogenic mutant as well as kinase-inhibited LRRK2. Conversely, addition of a non-hydrolyzable GTP analog to permeabilized cells enhances the association of pathogenic or kinase-inhibited LRRK2 with MTs. Our data elucidate the mechanism underlying the increased MT association of select pathogenic LRRK2 mutants or of pharmacologically kinase-inhibited LRRK2, with implications for downstream MT-mediated transport events.

Introduction

Parkinson's disease (PD) is a common neurodegenerative disease with incompletely understood etiology, affecting around 1–2% of the elderly (1). Mutations in the leucine-rich repeat kinase 2 (LRRK2) gene cause PD inherited in an autosomal-dominant fashion (2,3). Additionally, various variants have been identified which either positively or negatively correlate with PD risk (4–9), highlighting the general importance of LRRK2 for disease pathogenesis. The LRRK2 protein contains various domains implicated in protein–protein interactions, as well as a central region comprised of a Ras-of-complex (ROC) GTPase domain and a kinase domain, connected via a C-terminal of ROC

Received: February 19, 2017. **Revised:** April 17, 2017. **Accepted:** April 21, 2017

(COR) domain (10,11). All currently identified pathogenic mutants localize to this central region, and seem associated either with enhanced kinase activity (e.g. G2019S) (12–14), increased GTP binding (15–18) or reduced GTPase activity (19,20), suggesting that abnormal kinase and/or GTP-domain activities may cause neurodegeneration in LRRK2-linked PD (21). Indeed, pathogenic mutations in LRRK2 can promote cellular deficits through both GTP-dependent and kinase-dependent mechanisms (13,16,22–26), raising hopes that selective LRRK2 kinase inhibitors (27–29), GTP-binding competitors or GTPase modulators may delay the onset of LRRK2-related PD.

The precise mechanism(s) underlying LRRK2-linked PD remain largely unknown, but a variety of studies suggest underlying cytoskeletal alterations which may impact upon various vesicular trafficking steps (30). Endogenous LRRK2 protein can physically interact and colocalize with microtubules (MTs) (31–33). Such colocalization has also been observed with overexpressed LRRK2, and is profoundly enhanced with certain pathogenic LRRK2 mutants (34,35) as well as by several LRRK2 kinase inhibitors (36–38). Finally, pathogenic LRRK2 has been reported to impair MT-mediated axonal transport in a manner correlated with enhanced MT association (35,39). Thus, an increased interaction of LRRK2 with MTs seems to have detrimental effects on MT-mediated vesicular transport events. However, the molecular determinant(s) within LRRK2 required for such interaction are largely unknown.

Here, we have analyzed the subcellular localization of all pathogenic LRRK2 mutants as well as of pharmacologically kinase-inhibited LRRK2. We find that both mutant and kinase-inhibited LRRK2 preferentially interact with stable MTs. This interaction does not correlate with altered LRRK2 autophosphorylation status or kinase activity, but with enhanced GTP binding. Synthetic mutations in LRRK2 which reduce GTP binding, as well as two recently described GTP-binding inhibitors that attenuate LRRK2-mediated toxicity in cell and animal models (40,41) potently decrease this interaction, whilst a non-hydrolyzable GTP analog enhances the interaction. Thus, GTP-binding inhibitors may be useful for treating select forms of pathogenic LRRK2-linked PD.

Results

Kinase-inhibited LRRK2 and most pathogenic LRRK2 mutants display altered cellular localization

As previously described (34–38), GFP-tagged wild-type LRRK2 protein was found to adopt a purely cytosolic localization in the majority of transfected HEK293T cells (Fig. 1A). A small percentage of cells displayed additional dot-like localization in the form of one or several small, usually perinuclear structures, and a small percentage displayed a filamentous phenotype (Fig. 1A). Such localization was not tag-dependent, as also observed with myc-tagged LRRK2 constructs (not shown) (34).

The subcellular localization of LRRK2 may be modulated by either extrinsic and/or intrinsic factors. In support of the latter, pharmacological inhibition of LRRK2 kinase activity by either H1152 (36) or LRRK2-IN1 (37) has been reported to cause relocalization of LRRK2 to filamentous structures. Indeed, application of a whole set of specific and structurally distinct LRRK2 kinase inhibitors (37,42–46) triggered a profound relocalization of wild-type LRRK2 to filamentous structures (Fig. 1B) without causing alterations in steady-state protein levels (Fig. 1C). Relocalization was dose-dependent (Fig. 1D) and fast (Fig. 1E), being detectable within minutes after application of kinase inhibitor. Thus, pharmacological kinase inhibition invariably causes alterations in the subcellular localization of LRRK2.

We next evaluated the localization of all currently identified pathogenic LRRK2 mutants (N1437H, R1441C/G, Y1699C, I2012T, G2019S, I2020T) (2,3,17,47,48), as well as of two synthetic mutants known to either impair kinase activity (K1906M) or guanine nucleotide binding (K1347A), respectively. When compared with wild-type LRRK2, the filamentous phenotype was profoundly enhanced by all pathogenic LRRK2 mutants except for G2019S and I2012T (Fig. 1F and G). Both kinase-inactive and GTP-binding-deficient mutants displayed a primarily cytosolic localization (Fig. 1F and G), and all mutants with the exception of K1347A (26) were expressed to similar degrees (Fig. 1H), indicating that the observed differences in subcellular localization were not due to alterations in steady-state protein levels. Application of a LRRK2 kinase inhibitor (LRRK2-IN1) caused a further increase in filament formation of wild-type and all mutant LRRK2 proteins analyzed, but had no effect on synthetic kinase-inactive or GTP-binding-deficient mutants (Fig. 1G), suggesting that the latter two may be in a conformation incompatible with inhibitor binding (49,50). Thus, most pathogenic LRRK2 mutants display a profoundly altered subcellular localization, and pharmacological kinase inhibition further potentiates such relocalization for both wild-type as well as all currently identified pathogenic LRRK2 mutants.

LRRK2 filaments preferentially decorate stable MTs

The filamentous LRRK2 structures described here have been previously reported to colocalize with MTs (34,36). MTs are heterogeneous structures subject to distinct posttranslational modifications including acetylation and detyrosination (51–53), with the latter shown to cause increased MT stability (54). In non-transfected cells, the majority of the total MT array contained predominantly tyrosinated α-tubulin, indicative of dynamic MTs. Only a small subset of MTs was positive for acetylated and/or detyrosinated α-tubulin, with both posttranslational modifications frequently observed on the same MT tracks in a patchy, alternating fashion (Fig. 2A and B). Pathogenic as well as kinase inhibitor-induced LRRK2 filaments extensively colocalized with acetylated and/or detyrosinated α-tubulin, thus indicating a preference for association with stable MTs (Fig. 2A–C).

When compared with dynamic MTs, stable MTs display increased resistance to nocodazole, but are effectively disrupted upon cold treatment (55). Indeed, LRRK2 filaments were significantly disrupted upon cold treatment, with nocodazole being less effective (Fig. 3A). MT nucleation assays further revealed a delay between MT regrowth as assayed by staining against α-tubulin, the reformation of acetylated MTs, and the reformation of mutant LRRK2 filaments, in agreement with the preferential association of LRRK2 with stable MTs (Fig. 3B).

To examine whether modulating the acetylation and/or detyrosination status of MTs may influence the filamentous localization of pathogenic and kinase-inhibited LRRK2, we treated cells with two distinct α-tubulin deacetylase inhibitors (56) which increased the extent of tubulin acetylation and caused a modest decrease in the LRRK2 filamentous phenotype (Fig. 3C and D). As an alternative approach, we overexpressed αTAT1, the major α-tubulin acetyltransferase (57), which caused an increase in α-tubulin acetylation and a profound decrease in the pathogenic LRRK2 filamentous phenotype (Fig. 3E and F). An enzymatically inactive point mutant (D157N) (57) displayed

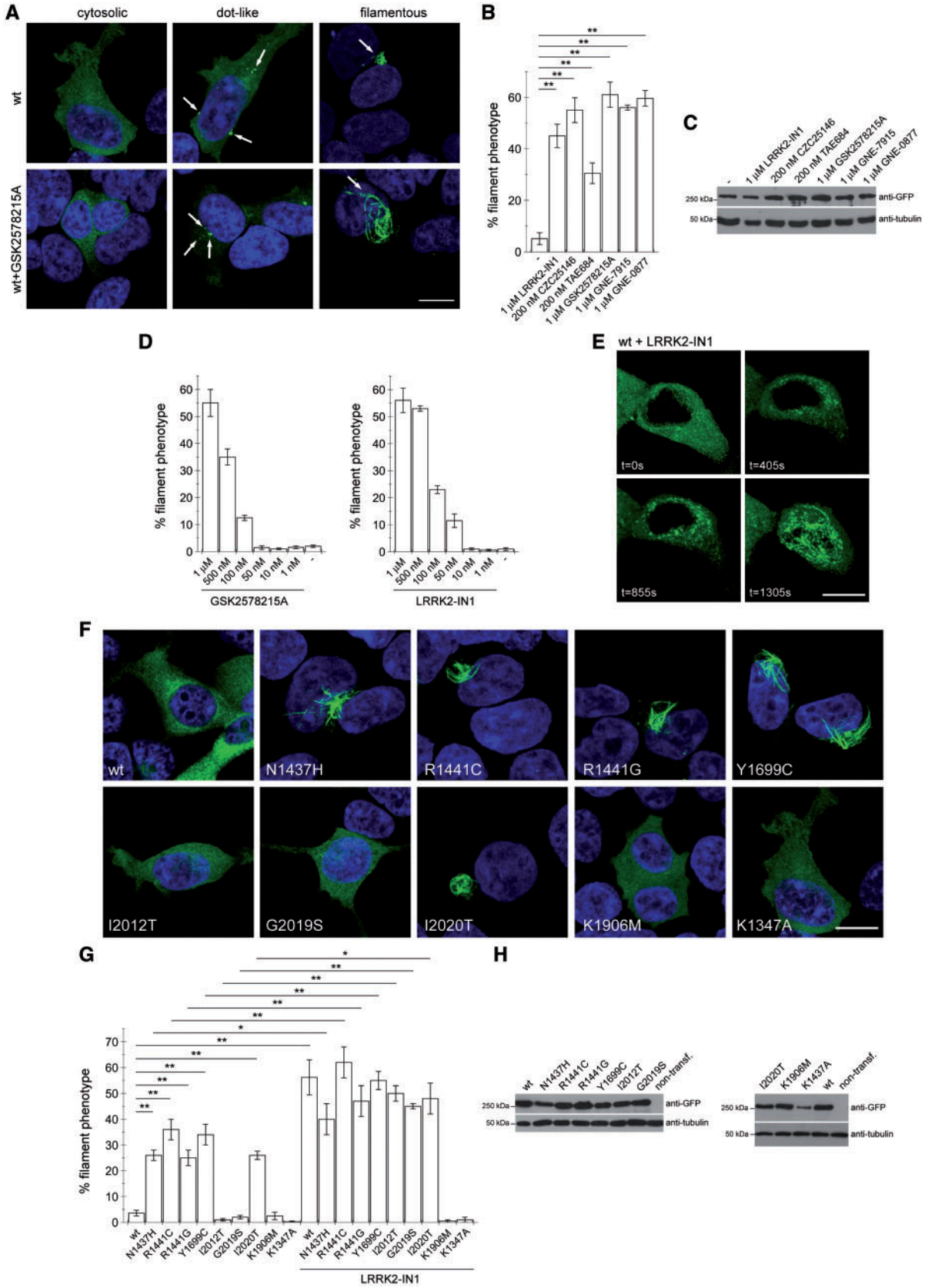

Figure 1. Effects of pharmacological kinase inhibitors and pathogenic mutations on LRRK2 subcellular localization. (**A**) Example of subcellular localization of wild-type GFP-tagged LRRK2 (wt) in the absence or presence of LRRK2 kinase inhibitor as indicated. Scale bar, 10 µm. (**B**) Quantification of the percentage of transfected cells displaying a filamentous phenotype in the absence of treatment (–), or upon 4 h incubation with distinct LRRK2 kinase inhibitors as indicated. Bars represent mean ± SEM

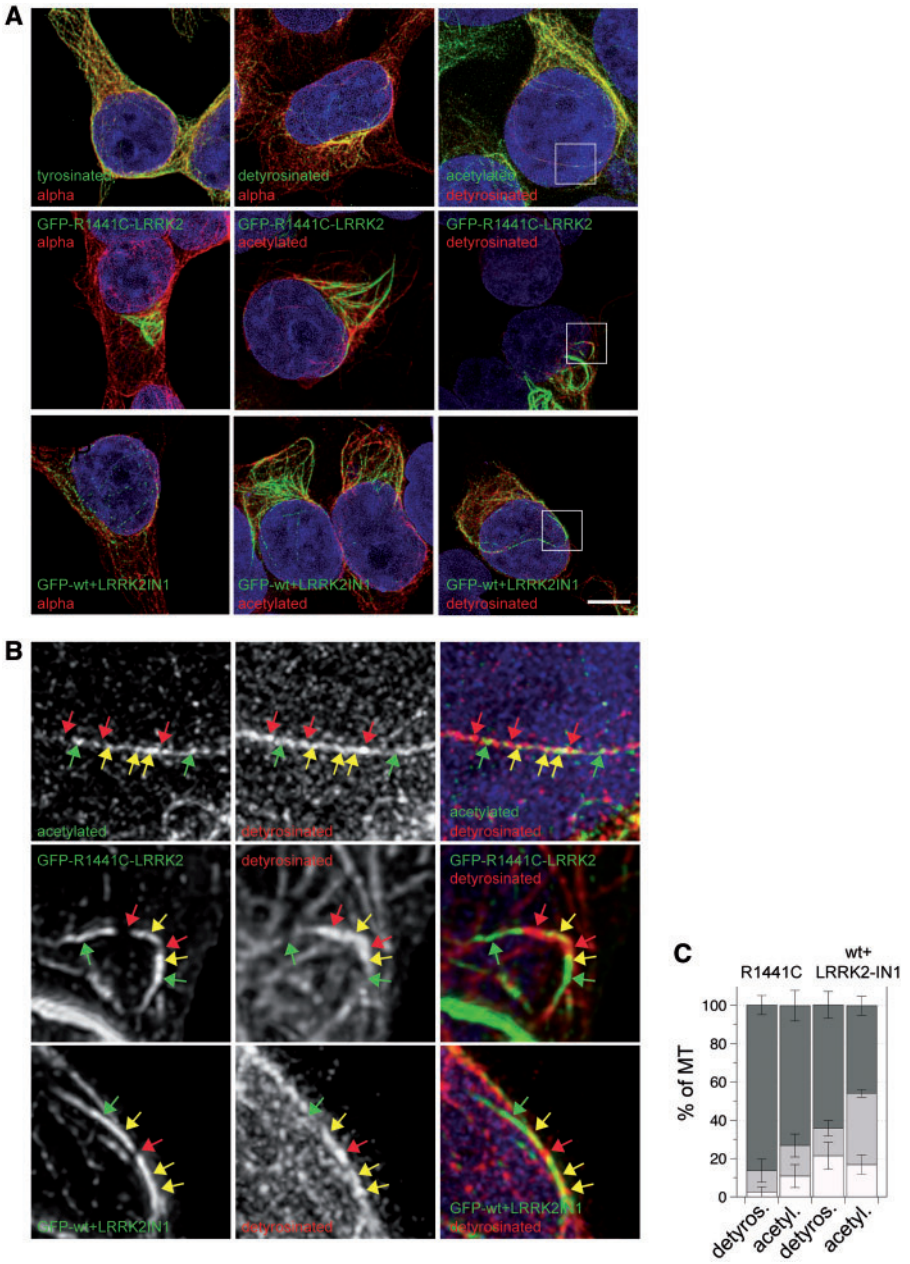

Figure 2. Pathogenic mutant and kinase-inhibited LRRK2 preferentially decorate stable MTs. (**A**) Example of non-transfected cells stained with antibodies against tyrosinated, detyrosinated, acetylated or α-tubulin (alpha) as indicated, or cells transfected with GFP-tagged R1441C-mutant LRRK2 and stained with antibodies as indicated, or cells transfected with GFP-tagged wild-type LRRK2, treated for 1 h with 1 μM LRRK2-IN1 and stained with antibodies as indicated. All images were deconvolved as described in Materials and Methods. Scale bar, 10 μm. (**B**) Magnification of squares as indicated in (A). Colored arrows indicate preferential staining with one antibody (red and green, respectively), or colocalization (yellow). (**C**) Quantification of colocalization of pathogenic mutant LRRK2 or wild-type LRRK2 in the presence of kinase inhibitor with either acetylated or detyrosinated MTs was performed as described in Materials and Methods. The percentage of colocalization was subgrouped for each cell, with colocalization 0–50% (white), 50–90% (gray) or > 90% (dark gray). Bars represent mean ± SEM ($n = 5$ cells).

Figure 1. Continued

($n = 3$; $^{**}P < 0.005$). (**C**) Cells were transfected with GFP-tagged wild-type LRRK2, treated with distinct kinase inhibitors for 4 h as indicated, and extracts analyzed for protein levels by western blotting using an anti-GFP antibody, and alpha-tubulin as loading control. (**D**) Quantification of the percentage of transfected cells displaying a filamentous phenotype in the absence (–) or presence of distinct concentrations of kinase inhibitors as indicated. Bars represent mean ± SEM ($n = 3$). (**E**) Live images of cells expressing wild-type GFP-tagged LRRK2 at distinct times after adding 1 μM LRRK2-IN1. Scale bar, 10 μm. (**F**) Examples of cells depicting the prominent subcellular localization of the various GFP-tagged LRRK2 constructs as indicated. Scale bar, 10 μm. (**G**) Quantification of the filamentous phenotype of various GFP-tagged LRRK2 constructs from the type of experiments as depicted in (F), in either the absence or presence of 1 μM LRRK2-IN1 for 4 h as indicated. Bars represent mean ± SEM ($n = 4$; $^{*}P < 0.05$; $^{**}P < 0.005$). (**H**) Cells were transfected with GFP-tagged LRRK2 constructs as indicated, and extracts analyzed for protein levels by western blotting using an anti-GFP antibody, and tubulin as loading control.

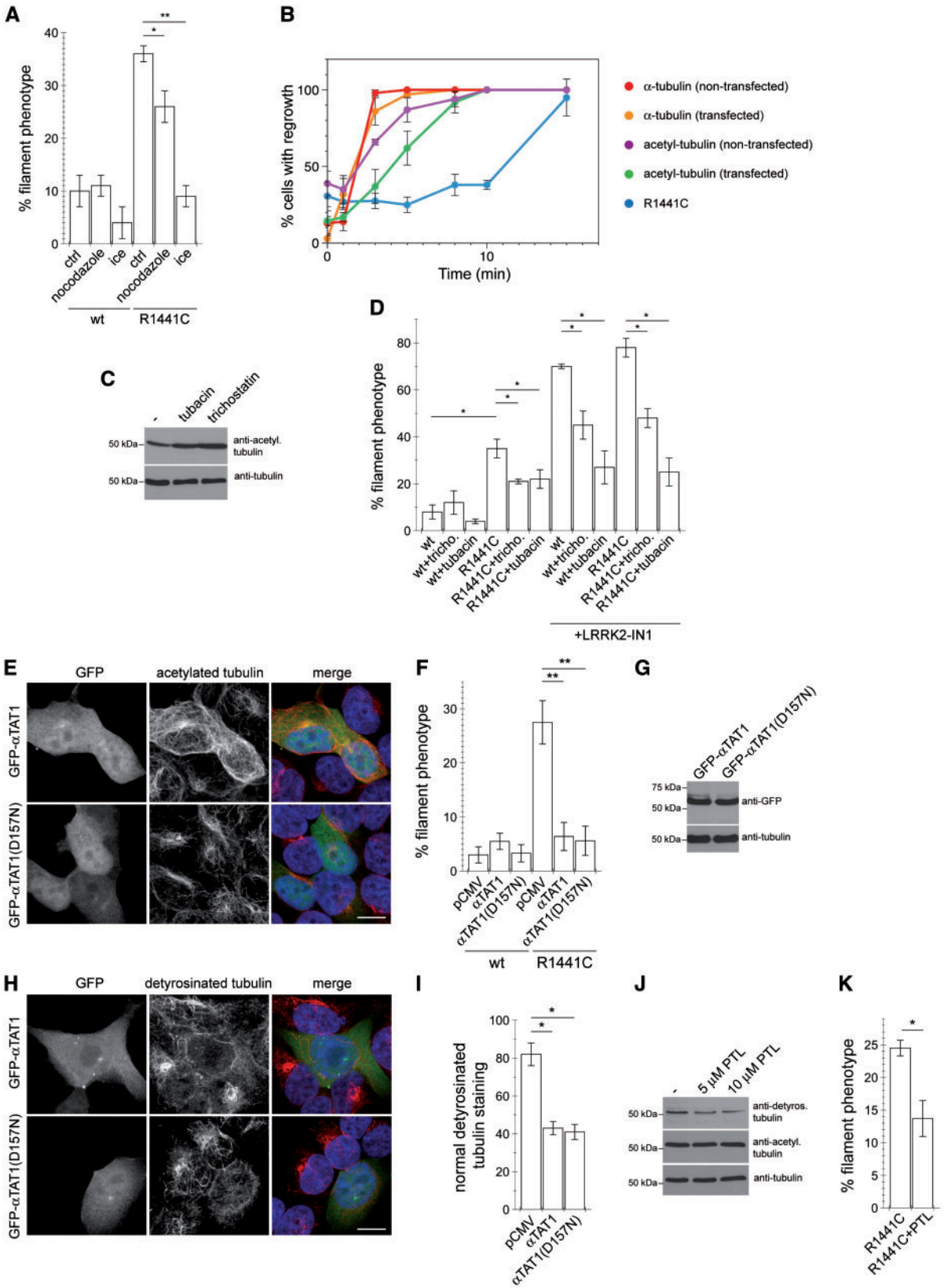

Figure 3. Effects of modulating the acetylation or detyrosination status of MTs on filament formation of pathogenic LRRK2. (A) Cells were transfected with constructs as indicated, and either left untreated (ctrl), or incubated with nocodazole or on ice, followed by quantification of the percentage of cells displaying a filamentous LRRK2 phenotype. Bars represent mean ± SEM ($n = 4$; *$P < 0.05$; **$P < 0.01$). (B) Cells were transfected with pathogenic LRRK2, incubated on ice for 1.5 h to disrupt MTs, and MT nucleation/regrowth performed for the indicated times at 37 °C. Cells were stained for α-tubulin or acetylated α-tubulin, and the percentage of non-transfected or transfected cells displaying visible MT regrowth and reformation of the filamentous pathogenic LRRK2 phenotype quantified as indicated. Bars represent

steady-state protein levels similar to wild-type αTAT1 (Fig. 3G), and was without effect on the acetylation status of α-tubulin (Fig. 3E). However, overexpression of the αTAT1 mutant defective in acetyltransferase activity also interfered with pathogenic LRRK2 filament formation, indicating that the observed effects were independent of MT acetylation status (Fig. 3F). Importantly, and as previously reported (58), expression of active and inactive αTAT1 both caused a decrease in detyrosinated α-tubulin (Fig. 3H and I), suggesting that LRRK2 filament formation may be largely modulated by the detyrosination status of MTs. Whilst the tubulin carboxypeptidase catalyzing the detyrosination of α-tubulin remains to be identified (53), parthenolide (PTL), a sesquiterpene lactone, has been shown to inhibit the activity of this enzyme (59,60). Indeed, treatment of cells with PTL caused a decrease in detyrosinated α-tubulin associated with a reduction in the filamentous phenotype of pathogenic mutant LRRK2 (Fig. 3J and K). Altogether, these results indicate that both pathogenic and kinase-inhibited LRRK2 preferentially associate with a subset of stable MTs in a manner mainly dependent on their detyrosination status.

LRRK2 filament formation does not correlate with kinase activity or autophosphorylation status

We next set out to identify the determinants within LRRK2 necessary for the observed MT interactions. Autophosphorylation of kinases is often used as a readout of enhanced kinase activity. LRRK2 has been shown to be autophosphorylated at various sites (61–65), with phosphorylation of one particular site (S1292) detectable *in vivo* and increased in the context of various pathogenic mutants (38). As previously reported (38), when introduced into a combined pathogenic mutant background (R1441C-Y1699C-G2019S), the S1292A mutation decreased the LRRK2 filamentous phenotype (Fig. 4A). However, when introduced into constructs bearing the individual pathogenic LRRK2 mutations, no change in their subcellular localization was observed (Fig. 4B), with all mutants expressed to similar degrees (Fig. 4C). Thus, enhanced S1292 autophosphorylation does not seem to comprise a relevant molecular determinant required for the observed filamentous phenotype of pathogenic LRRK2 mutants.

A series of distinct pharmacological kinase inhibitors caused filament formation, whilst a kinase-inactive point mutant (K1906M) did not (Fig. 1). Pharmacological kinase inhibition has been suggested to induce a conformational change in LRRK2 associated with dephosphorylation of the cellular N-terminal phosphorylation sites including S935, which was not observed with kinase-dead point mutants (50). Indeed, two distinct kinase-dead point mutants (K1906M and T2035A) displayed N-terminal phosphorylation levels similar to wild-type LRRK2 (Fig. 5A and B). Pharmacological kinase inhibition of wild-typEe LRRK2 caused dephosphorylation of the N-terminal S935 residue, which was also observed when adding pharmacological kinase inhibitor to kinase-dead T2035A, but not to the K1906M mutant, respectively (Fig. 5A and B). The changes in N-terminal dephosphorylation correlated with filament formation in pharmacologically kinase-inhibited wild-type and T2035A mutant LRRK2, with K1906M mutant LRRK2 not showing dephosphorylation neither filament formation upon pharmacological kinase inhibition (Fig. 5C). Therefore, synthetic kinase-dead LRRK2 mutants do not seem to properly mimick the features of pharmacologically kinase-inhibited LRRK2, with the latter being accompanied by a change associated with dephosphorylation of the N-terminal cellular phosphorylation sites.

The filamentous localization of LRRK2 is modulated by 14-3-3

Interestingly, N-terminal phosphorylation is also decreased in pathogenic LRRK2 mutants which display a filamentous phenotype, but not in the G2019S mutant which is largely cytosolic (36,66,67) (Fig. 5D). Since dephosphorylation of the cellular N-terminal phosphorylation sites causes disruption of 14-3-3 binding (66,67), and since overexpression of 14-3-3 proteins has been found to ameliorate the effects of pathogenic LRRK2 on neurite length (68), we next wondered whether 14-3-3 protein overexpression may alter the filamentous phenotype and N-terminal phosphorylation status of LRRK2. Overexpression of either 14-3-3β or 14-3-3γ, both reported to interact with LRRK2 (69,70), decreased the filamentous phenotype of pathogenic LRRK2 without altering its dot-like localization (Fig. 6A and B). In addition, expression of either 14-3-3 protein decreased the filamentous phenotype of wild-type or pathogenic LRRK2 induced upon pharmacological kinase inhibition (Fig. 6B). In contrast, whilst expressed to a similar degree (Fig. 6C), a loss-of-function point mutant (V181D) of 14-3-3γ (70) was without effect (Fig. 6B). Overexpression of wild-type but not mutant 14-3-3γ was associated with an increase in N-terminal phosphorylation of pathogenic mutant LRRK2 similar to that observed with wild-type LRRK2 (Fig. 6D). Therefore, modulating cellular 14-3-3 levels with concomitant effects on the N-terminal phosphorylation status of LRRK2 seems to modulate filament formation.

We next wondered whether abolishing N-terminal phosphorylation may be sufficient to cause the observed filamentous phenotype of pathogenic and pharmacologically kinase-inhibited LRRK2. Preventing N-terminal phosphorylation by mutating S935 or S910/S935, either in the presence or absence of additional mutations in S955 and S973 caused increased dot-like localization (66,67) (Fig. 7A), but had no effect on the filamentous phenotype in either the absence or presence of LRRK2 kinase inhibitor (Fig. 7B), with all mutants expressed to similar degrees (Fig. 7C). Similarly, mutating another phosphorylation

Figure 3. Continued

mean ± SEM ($n = 4$ experiments). (**C**) Cells were left either untreated (–) or treated with tubacin or trichostatin A as indicated, and extracts analyzed for levels of acetylated α-tubulin and total α-tubulin as loading control. (**D**) Cells were transfected with the indicated constructs, left untreated or incubated with trichostatin A (tricho.) or tubacin either in the presence or absence of 1 μM LRRK2-IN1 for 4 h, and the percentage of cells displaying a filamentous phenotype quantified. Bars represent mean ± SEM ($n = 3$; $^{*}P < 0.05$). (**E**) Cells were transfected with GFP-tagged wild-type αTAT1 or an inactive point mutant (D157N) as indicated, followed by staining with an antibody against acetylated α-tubulin. Scale bar, 10 μm. (**F**) Cells were co-transfected with either GFP-tagged wild-type or R1441C-mutant LRRK2 and empty control vector (pCMV) or RFP-tagged wild-type or mutant αTAT1 as indicated, followed by quantification of the percentage of cells displaying a filamentous LRRK2 phenotype. Bars represent mean ± SEM ($n = 3$; $^{**}P < 0.01$). (**G**) Cells were transfected with GFP-tagged wild-type or mutant αTAT1 as indicated, and extracts analyzed for protein levels with α-tubulin as loading control. (**H**) Cells were transfected with GFP-tagged wild-type αTAT1 or an inactive point mutant (D157N) as indicated, followed by staining with an antibody against detyrosinated α-tubulin. Scale bar, 10 μm. (**I**) Cells were transfected with wild-type or mutant αTAT1 as indicated, and the percentage of transfected cells with visibly abnormal detyrosinated α-tubulin staining quantified. Bars represent mean ± SEM ($n = 3$; $^{*}P < 0.05$). (**J**) Cells were left either untreated (–), or treated with different concentrations of parthenolide (PTL) for 12 h as indicated, and extracts analyzed for levels of detyrosinated, acetylated and total α-tubulin. (**K**) Cells were transfected with R1441C-mutant LRRK2, treated for 12 h with PTL as indicated, followed by quantification of the percentage of cells displaying a filamentous LRRK2 phenotype. Bars represent mean ± SEM ($n = 3$; $^{*}P < 0.05$).

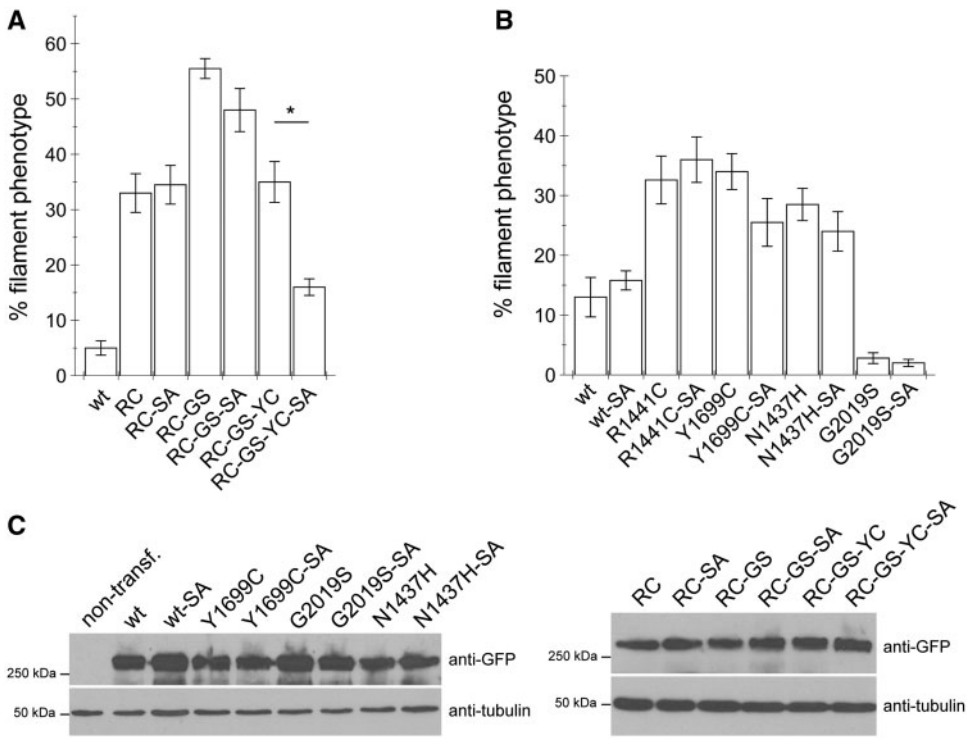

Figure 4. Alterations in autophosphorylation status of LRRK2 on S1292 does not correlate with filamentous phenotype. (**A**) Cells were transfected with the indicated constructs, followed by quantification of the percentage of cells displaying a filamentous phenotype. Bars represent mean ± SEM ($n = 5$; $^*P < 0.05$). (**B**) Cells were transfected with the indicated constructs, followed by quantification of the percentage of cells displaying a filamentous phenotype. Bars represent mean ± SEM ($n = 5$). (**C**) Cells were transfected with GFP-tagged LRRK2 constructs as indicated, and extracts analyzed for protein levels by western blotting using an anti-GFP antibody, and tubulin as loading control.

site in the ROC domain in conjunction with S910, both previously reported to be important for 14-3-3 binding (71) caused increased dot-like localization of wild-type LRRK2 (Fig. 7D), but had no effect on the filament phenotype (Fig. 7E), with similar steady-state protein levels of all mutants examined (Fig. 7C). Thus, mimicking lack of phosphorylation of sites involved in 14-3-3 binding is not sufficient to mimick the filamentous phenotype observed with mutant or pharmacologically kinase-inhibited LRRK2.

Mutations within the catalytic switch II motif of the ROC GTPase domain impair the filamentous localization of pathogenic and kinase-inhibited LRRK2

Apart from altered kinase activity, altered GTP binding and/or GTPase activity have been implicated in LRRK2-related pathogenesis (16,23–26,40,41,72,73). The GTPase activity of LRRK2 has been reported to be modulated by GTPase activating proteins (GAPs) including ArfGAP1 and RGS2, and guanine nucleotide exchange factors (GEFs) such as ARHGEF7 (24,25,74,75). Co-expression of either ArfGAP1 or RGS2 with wild-type or pathogenic R1441C-mutant LRRK2 was without effect on the filamentous phenotype of LRRK2 in the absence or presence of kinase inhibitors (Fig. 8A and B). ARHGEF7 significantly decreased wild-type LRRK2 filament formation triggered by pharmacological kinase inhibition, and also decreased filament formation of pathogenic LRRK2 in the absence or presence of kinase inhibitors (Fig. 8C). However, an inactive GEF-dead variant (L386R/L387S) (75), expressed to similar degrees, also effectively interfered with filament formation (Fig. 8C and D). As the binding of ARHGEF7 to LRRK2 is independent on the guanine nucleotide exchange activity of ARHGEF7 (75), the observed effects of both active and inactive ARHGEF7 are likely due to competing for the same binding site(s) on LRRK2 as those required for MT interactions, rather than due to effects related to ARGEF7-mediated alterations of the GTPase activity of LRRK2.

As an alternative approach to probe for the effect of LRRK2 GTP binding on filament formation, we generated a set of synthetic mutations. Previous structural studies have suggested that two residues in the ROC domain of LRRK2 (R1398 and T1343) may be important for interaction with the γ-phosphate of GTP (76). In addition, mutating R1398 has been described to decrease LRRK2 GTP binding, with a further decrease observed when additionally mutating T1343 (23), and both R1398L and R1398L/T1343V mutations have been reported to largely revert the effects of pathogenic LRRK2 on neurite outgrowth, all whilst having no detrimental effects on protein stability and/or structure (26). We thus wondered whether these mutations may alter the pathogenic LRRK2 filamentous phenotype. When introduced into wild-type or G2019S-mutant LRRK2, no effect on filament formation was observed with either R1398L (RL), T1343V (TV) or R1398L/T1343V (RLTV) mutations (Fig. 8E). However, the RL mutation caused a significant decrease in filament formation in the context of all pathogenic filament-forming LRRK2 mutants (N1437H, R1441C, Y1699C and I2020T) (Fig. 8F and G). Whilst the TV mutation was not displaying an effect on its own when introduced into wild-type or the various pathogenic LRRK2 mutants, the combination of both synthetic mutations (RLTV) drastically decreased the filamentous phenotype of pathogenic N1437H, R1441C, Y1699C and I2020T LRRK2, with all the various proteins expressed to similar degrees (Fig. 8F–H).

Importantly, the RLTV mutation also decreased filament formation of wild-type and pathogenic LRRK2 mutants upon pharmacological kinase inhibition (Fig. 8E–G), indicating a shared mechanism underlying the altered localization of pathogenic mutant and kinase-inhibited LRRK2.

Various reports indicate that an R1398H polymorphism in LRRK2 is associated with decreased PD risk (6–9). Similar to the R1398L mutation, the protective R1398H (RH) mutation reduced the filamentous phenotype of pathogenic LRRK2 in the absence or presence of kinase inhibitors, and this effect was not due to altered steady-state protein levels (Fig. 9A and B). Thus, select mutations in the switch II region of the ROC domain of LRRK2, including a protective risk variant, profoundly decrease the filamentous localization of pathogenic as well as kinase-inhibited LRRK2.

Altered subcellular localization of pathogenic and kinase-inhibited LRRK2 correlates with increased GTP binding and can be reverted by select LRRK2 GTP-binding inhibitors

As the synthetic mutations in the ROC domain are predicted to interfere with GTP binding (76), we measured steady-state GTP binding capacity of pathogenic mutant or pharmacologically kinase-inhibited LRRK2. As previously reported, addition of LRRK2 kinase inhibitors caused a significant increase in GTP binding of wild-type LRRK2 (77) (Fig. 10A and B), whilst the K1347A mutation, known to disrupt the guanine nucleotide-binding P-loop motif, almost completely abolished GTP binding (16,26) (Fig. 10C and D). All filament-forming pathogenic mutants displayed enhanced GTP binding when compared with wild-type LRRK2 (Fig. 10C and D), whilst the RL mutation, and to a larger degree the RLTV mutation, caused a drastic decrease in steady-state GTP binding of wild-type and all pathogenic mutants (Fig. 10E and F). Similarly to the RL mutation, and as previously described in the context of wild-type LRRK2 (78), the protective R1398H variant also displayed a decrease in GTP binding of wild-type and all pathogenic LRRK2 mutants (Fig. 10G).

The capacity for GTP binding may be important for LRRK2 kinase activity (79). Therefore, we next tested the effects of the RL and RLTV mutations on LRRK2 kinase activity. Of all mutants analyzed, only G2019S caused a significant, around 3-fold increase in LRRK2 kinase activity, in agreement with previous studies (80,81) (Fig. 11A and B). The RLTV mutation significantly decreased kinase activity of wild-type and most pathogenic LRRK2 mutants, whilst the RL mutation showed little effect on kinase activity (Fig. 11A and B), even though both RL and RLTV mutants interfered with the filamentous LRRK2 phenotype (Fig. 8E–G). These results indicate that the altered subcellular localization of mutant or pharmacologically kinase-inhibited LRRK2 correlates with enhanced GTP binding rather than with alterations in LRRK2 kinase activity.

Recent studies have described the identification of several LRRK2 GTP-binding inhibitors able to attenuate LRRK2 toxicity, and able to rescue vesicular transport deficits associated with impaired neurite outgrowth (39–41). Both compound 68 and compound 70 significantly reduced LRRK2 GTP binding *in vitro* (Fig. 12A and B). Importantly, these compounds also reverted the filamentous phenotype of both pathogenic and pharmacologically kinase-inhibited LRRK2 (Fig. 12C and D). Conversely, addition of a non-hydrolyzable GTP analog to transiently permeabilized cells enhanced the filamentous phenotype of pathogenic or kinase-inhibited LRRK2 (Fig. 12E), providing further and direct evidence for the importance of GTP binding as a crucial molecular determinant for LRRK2 filament formation.

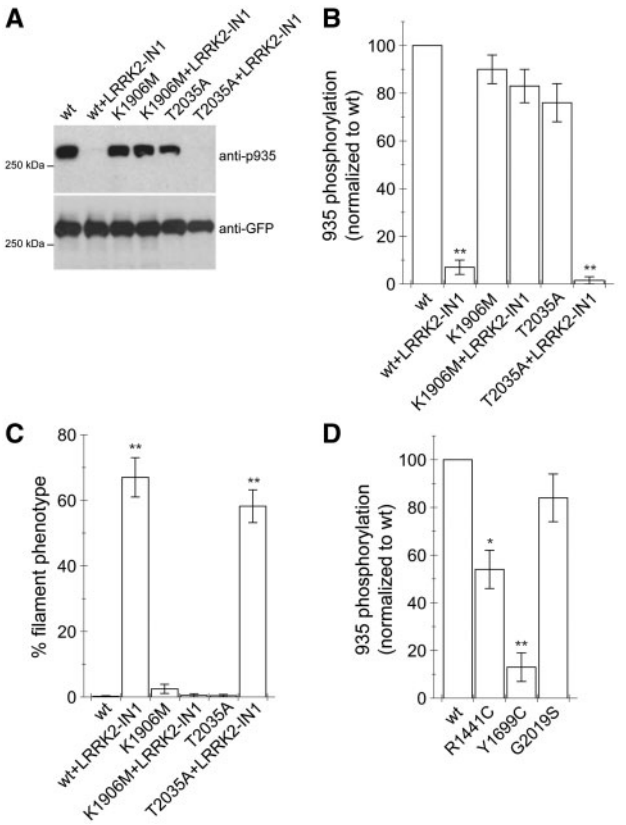

Figure 5. Differential dephosphorylation of cellular N-terminal phosphorylation sites correlates with filamentous phenotype in pharmacologically kinase-inhibited, synthetic kinase-dead and pathogenic mutant LRRK2. (**A**) Cells were transfected with the indicated constructs, and either left untreated or incubated with 1 μM LRRK2-IN1 for 4 h as indicated, and extracts analyzed for phosphorylated (S935) or total (GFP) GFP-tagged LRRK2 as indicated. (**B**) Quantification of the type of experiments depicted in A, with phospho-S935 signals normalized to those found in wild-type LRRK2. Bars represent mean ± SEM ($n = 3$; $^{**}P < 0.01$). (**C**) Cells were transfected with the indicated constructs, and either left untreated or incubated with 1 μM LRRK2-IN1 for 4 h as indicated, followed by quantification of the percentage of transfected cells displaying a filamentous phenotype. Bars represent mean ± SEM ($n = 4$; $^{**}P < 0.001$). (**D**) Cells were transfected with the indicated constructs, extracts analyzed for phosphorylated (S935) or total (GFP) GFP-tagged LRRK2 as indicated, and phospho-S935 signals normalized to wild-type LRRK2. Bars represent mean ± SEM ($n = 3$; $^{**}P < 0.01$; $^{*}P < 0.05$).

Finally, to determine the relative importance of altered N-terminal phosphorylation to the observed filamentous phenotype, we analyzed the phosphorylation of the N-terminal S935 residue in wild-type or pathogenic mutant LRRK2 in the absence or presence of the RL, the RLTV, or the protective RH mutation (Fig. 13A and B). The presence of mutations shown to cause a decrease in GTP binding and filament formation did not display altered S935 phosphorylation when compared with their respective non-mutant counterparts (Fig. 13A and B). Similarly, GTP-binding inhibitors which decrease GTP binding and partially revert the filamentous phenotype caused no effect on S935 phosphorylation of pharmacologically kinase-inhibited or pathogenic mutant LRRK2, respectively (Fig. 13C), and GTP analogs which increase filament formation did not change S935 phosphorylation of either pathogenic or pharmacologically kinase-inhibited LRRK2 (Fig. 13D). Since increasing cellular 14-3-

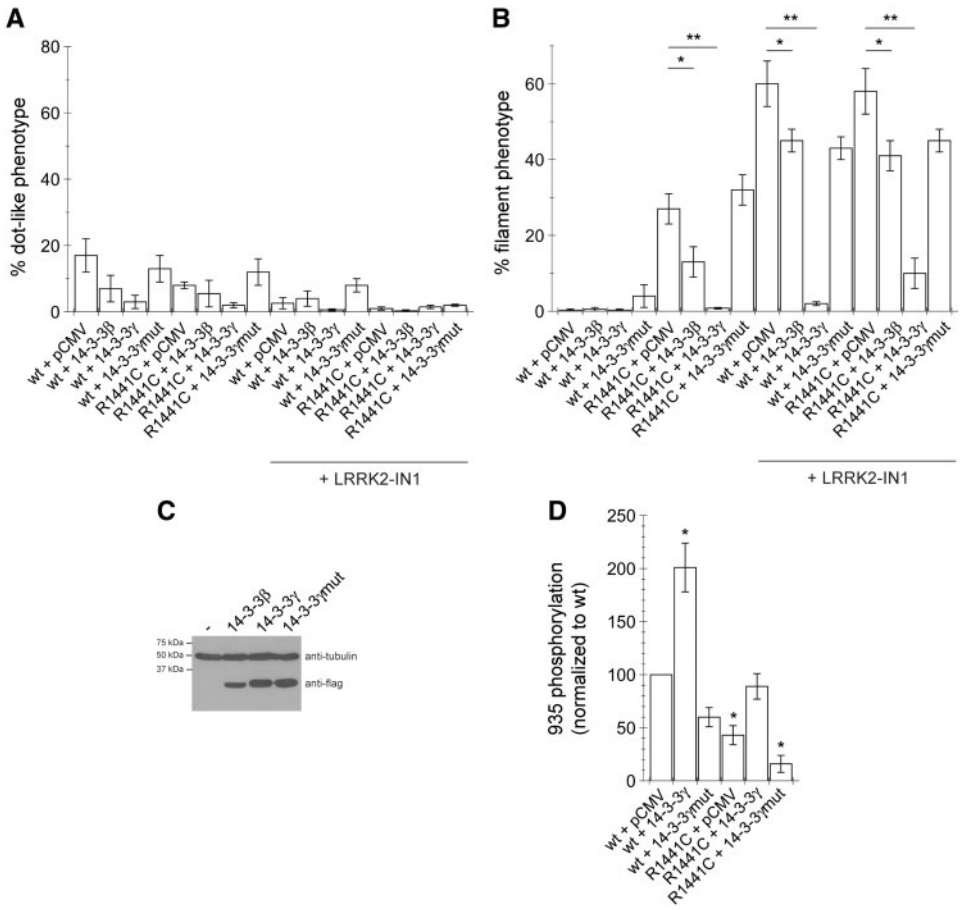

Figure 6. Overexpression of 14-3-3 alters filamentous LRRK2 phenotype and N-terminal phosphorylation status. (**A**) Cells were transfected with the indicated constructs, and either left untreated or incubated with 1 μM LRRK2-IN1 for 4 h, followed by quantification of the percentage of transfected cells displaying a dot-like LRRK2 phenotype. (**B**) Same as in (A), but quantifying the percentage of cells displaying a filamentous phenotype. Bars represent mean ± SEM ($n = 3$; $^*P < 0.05$; $^{**}P < 0.005$). (**C**) Cells were transfected with flag-HA-tagged constructs as indicated, and extracts analyzed for protein levels by western blotting using an anti-flag antibody, and tubulin as loading control. (**D**) Cells were transfected with the indicated constructs, extracts analyzed for phosphorylated (S935) or total (GFP) GFP-tagged LRRK2 as indicated, and phospho-S935 signals normalized to wild-type LRRK2. Bars represent mean ± SEM ($n = 3$; $^*P < 0.05$).

3 levels with a concomitant increase in the N-terminal phosphorylation status of pathogenic LRRK2 was found to decrease the filamentous phenotype of pathogenic LRRK2 (Fig. 6), we analyzed whether this correlated with altered GTP binding. Indeed, the presence of wild-type, but not of loss-of-function mutant 14-3-3γ, caused a decrease in LRRK2 GTP binding (Fig. 13E). Therefore, whilst changes in the N-terminal phosphorylation status can parallel the observed alterations in the subcellular localization of pathogenic or pharmacologically kinase-inhibited LRRK2, they do not seem to be necessary to cause such phenotype. Rather, the key molecular determinant underlying the filamentous phenotype of pathogenic or pharmacologically kinase-inhibited LRRK2 relates to altered GTP binding.

Discussion

Various independent studies have reported that LRRK2 interacts with MTs, even though a preferential association with dynamic versus stable MTs has remained unclear (31,33–35). Whilst the presence of LRRK2 in growth cones has been taken to indicate that it may preferentially interact with dynamic MTs (39), such localization may be contributed to by additional factors. Furthermore, the previously reported alternating nature between the presence of pathogenic LRRK2 and acetylated α-tubulin staining has been taken as evidence that it interacts with dynamic MTs (35), but our data suggest this to be an unlikely interpretation for several reasons. Firstly, only a small subset of all MTs display posttranslational modifications including detyrosination and acetylation, and compared with colocalization with α-tubulin or tyrosinated α-tubulin, we observed a high degree of colocalization of mutant and kinase-inhibited LRRK2 with only the small subset of detyrosinated and/or acetylated MTs. Furthermore, detyrosination and acetylation can often be observed on the same tracks in a 'patchy' fashion (82), reminiscent of the colocalization of LRRK2 with MT tracks which are either detyrosinated and/or acetylated. Finally, decreasing detyrosination by various means interfered with the filamentous LRRK2 phenotype. Whilst some of the data have to be interpreted with care due to the likely lack of compound selectivity (53), they are consistent with the idea that modulation of posttranslational tubulin modifications can impact upon the interaction of mutant and kinase-inhibited LRRK2 with stable MTs.

Both acetylation and detyrosination are generally enriched on stable MTs, but the contribution of acetylation to MT stability remains unclear (53), whilst detyrosination has been clearly reported to protect MTs from the depolymerizing activity of certain motor proteins, thereby increasing their longevity (54).

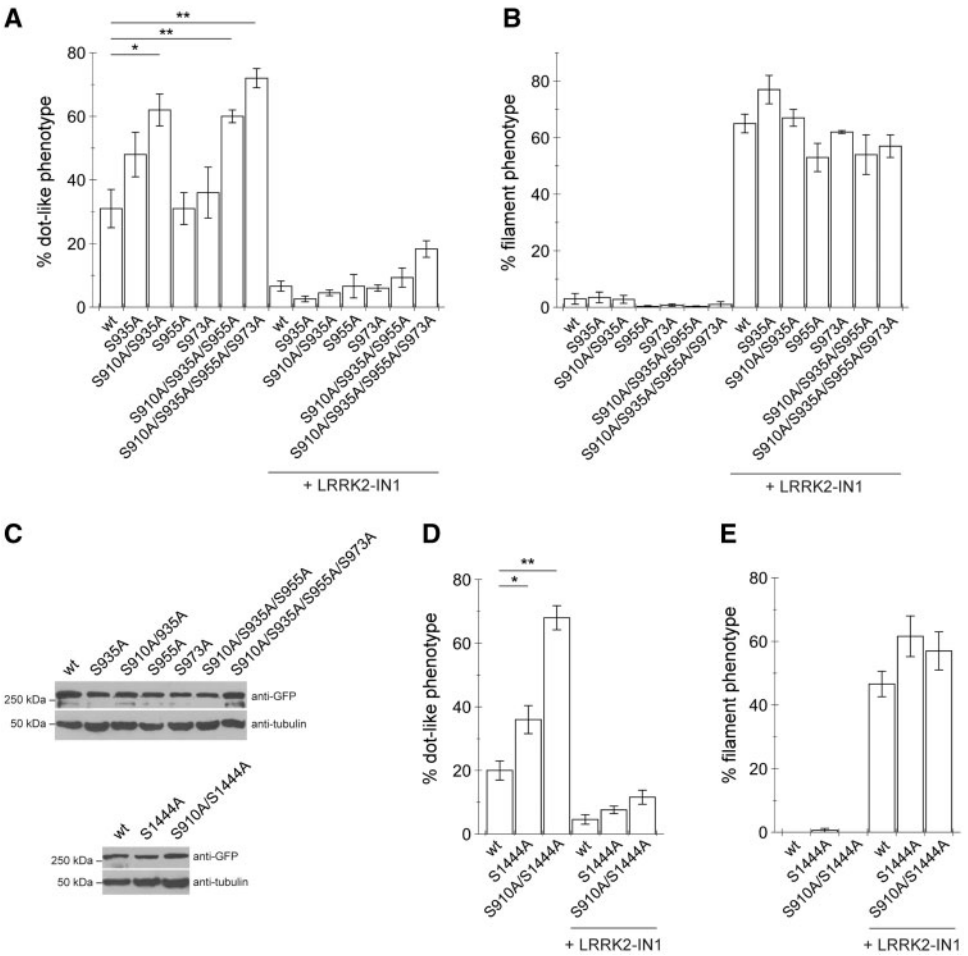

Figure 7. Mutations of the LRRK2 cellular phosphorylation sites do not cause a filamentous phenotype. (**A**) Cells were transfected with the indicated constructs, and either left untreated or incubated with 1 μM LRRK2-IN1 for 4 h as indicated, followed by quantification of the percentage of transfected cells displaying a dot-like LRRK2 phenotype. Bars represent mean ± SEM ($n = 4$; $^{*}P < 0.01$; $^{**}P < 0.005$). (**B**) Same as in (A), but quantifying the percentage of cells displaying a filamentous phenotype. (**C**) Cells were transfected with GFP-tagged LRRK2 constructs as indicated, and extracts analyzed for protein levels by western blotting using an anti-GFP antibody, and tubulin as loading control. (**D**) Cells were transfected with the indicated constructs, and either left untreated or incubated with 1 μM LRRK2-IN1 for 4 h as indicated, followed by quantification of the percentage of transfected cells displaying a dot-like LRRK2 phenotype. Bars represent mean ± SEM ($n = 4$; $^{*}P < 0.05$; $^{**}P < 0.005$). (**E**) Same as in (D), but quantifying the percentage of cells displaying a filamentous phenotype.

Apart from contributing to MT stability, posttranslational tubulin modifications are also recognized by different molecular motor proteins, and this contributes to the establishment and maintenance of polarized vesicular trafficking (83–85). Therefore, enhanced interactions of pathogenic and kinase-inhibited LRRK2 with stable MTs may interfere with select vesicular trafficking events such as the kinesin-mediated transport along stable axonal MTs (85,86). In support of this possibility, pathogenic LRRK2-mediated axonal vesicular transport deficits have been consistently reported in various experimental model systems (35,39,87,88), and synaptic and axonal degeneration are observed in postmortem brains of PD patients (89). In sum, currently available data are consistent with the LRRK2-MT interaction occurring on a subpopulation of stable MTs, with possible downstream effects on MT-mediated vesicular transport events.

The precise molecular determinants within LRRK2 required for MT interactions have remained unknown. Here, we found that all pathogenic LRRK2 mutants with the exception of G2019S and I2012T showed enhanced colocalization with MTs. When assayed *in vitro*, only G2019S has been consistently reported to display increased kinase activity (80,81), with I2012T showing a decrease (14), and pathogenic mutants in the ROC–COR domain showing no change when compared with wild-type LRRK2, respectively. Thus, the altered subcellular localization of the various pathogenic LRRK2 mutants does not seem to correlate with their inherent differences in kinase activity as determined *in vitro*.

As another means to gauge for a possible correlation between altered kinase activity and filament formation, we determined the impact of abolishing autophosphorylation on this cellular readout. Like many other protein kinases, LRRK2 is subject to autophosphorylation (38,61–65). Amongst a variety of identified sites, autophosphorylation at S1292 has been detected *in vivo*, and a S1292A mutation has been reported to substantially reduce the filamentous localization of a LRRK2 variant harboring two distinct pathogenic mutations within the same molecule (38). Whilst we did corroborate a decrease in the filamentous phenotype of a LRRK2 variant harboring multiple pathogenic mutations, abolishing this autophosphorylation site in the context of the individual pathogenic mutants was without effect on their subcellular localization. We cannot exclude

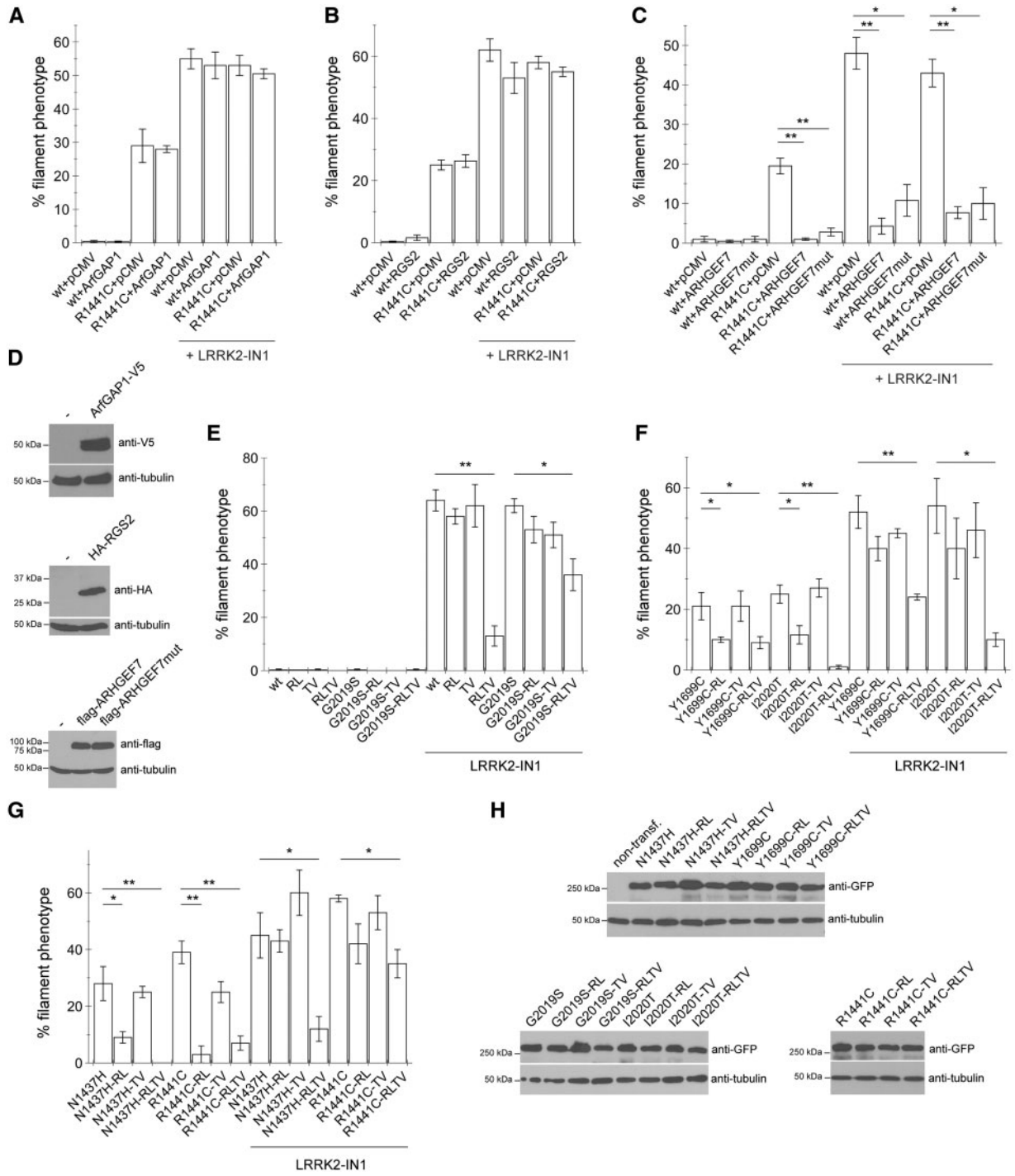

Figure 8. Mutations in the catalytic switch II motif impair the filamentous phenotype of pathogenic and kinase-inhibited LRRK2. (**A**) Cells were transfected with either wild-type or pathogenic LRRK2 along with ArfGAP1, left untreated or incubated in the presence of 1 μM LRRK2-IN1 for 4 h as indicated, and the percentage of cells displaying a filamentous phenotype quantified. Bars represent mean ± SEM ($n = 3$). (**B**) Cells were transfected with either wild-type or pathogenic LRRK2 along with RGS2, left untreated or incubated in the presence of 1 μM LRRK2-IN1 for 4 h as indicated, and the percentage of cells displaying a filamentous phenotype quantified. Bars represent mean ± SEM ($n = 4$). (**C**) Cells were transfected with either wild-type or pathogenic LRRK2 along with ARHGEF7 or inactive variant (ARHGEF7mut), left untreated or incubated in the presence of 1 μM LRRK2-IN1 for 4 h as indicated, and the percentage of cells displaying a filamentous phenotype quantified. Bars represent mean ± SEM ($n = 3$; $^*P < 0.05$; $^{**}P < 0.01$). (**D**) Cells were transfected with tagged constructs as indicated, and extracts analyzed for protein levels by western blotting, with tubulin as loading control. (**E**) Cells were transfected with the indicated LRRK2 variants, left untreated or incubated in the presence of 1 μM LRRK2-IN1 for 4 h, and the percentage of cells displaying a filamentous phenotype quantified. Bars represent mean ± SEM ($n = 3$; $^*P < 0.05$; $^{**}P < 0.01$). (**F**) As in (**E**). Bars represent mean ± SEM ($n = 3$; $^*P < 0.05$; $^{**}P < 0.01$). (**G**) As in (**E**). Bars represent mean ± SEM ($n = 3$; $^*P < 0.05$; $^{**}P < 0.01$). (**H**) Cells were transfected with the indicated GFP-tagged constructs, and extracts analyzed for protein levels by western blotting, with tubulin as loading control.

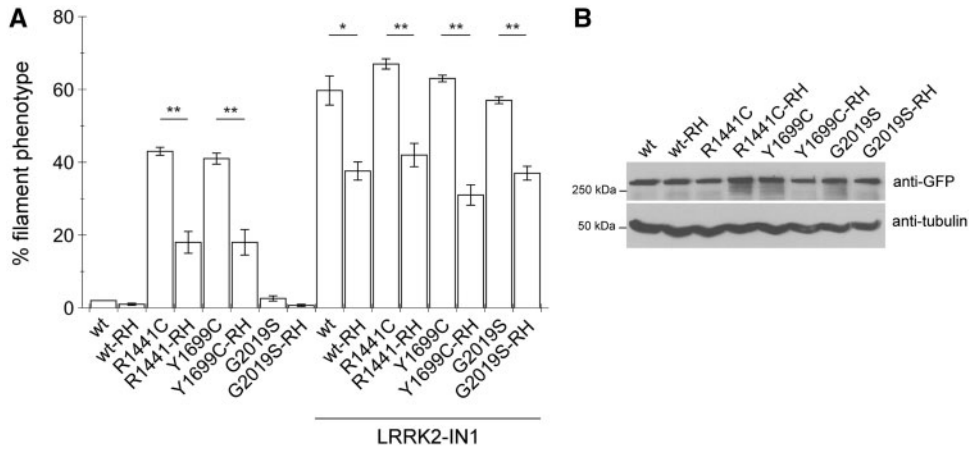

Figure 9. The protective R1398H PD risk variant decreases the filamentous LRRK2 phenotype. (**A**) Cells were transfected with the indicated constructs, left untreated or incubated in the presence of 1 μM LRRK2-IN1 for 4 h, and the percentage of cells displaying a filamentous phenotype quantified. Bars represent mean ± SEM ($n = 3$; $^{*}P < 0.05$; $^{**}P < 0.005$). (**B**) Cells were transfected with the indicated GFP-tagged constructs, and extracts analyzed for protein levels by western blotting, with tubulin as loading control.

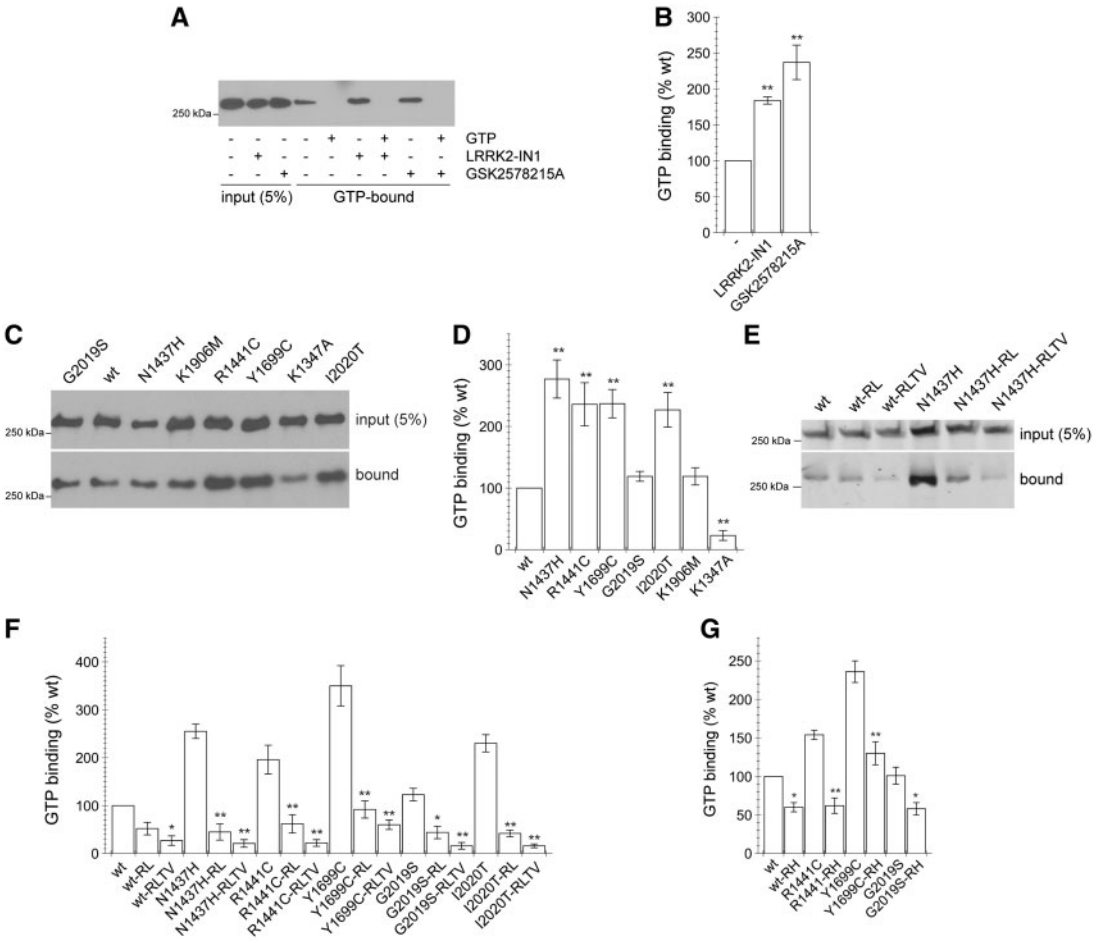

Figure 10. Pathogenic mutant or pharmacologically kinase-inhibited LRRK2 display enhanced GTP binding, and both RL and RLTV mutations cause a decrease in LRRK2 GTP binding. (**A**) Transfected HEK293T cells were incubated with either 1 μM LRRK2-IN1 or 1 μM GSK2578215A for 4 h as indicated, LRRK2 was affinity-purified from lysates using GTP-agarose in the presence of kinase inhibitors, and input (5%) and GTP-bound protein subjected to western blot analysis using an anti-GFP antibody. (**B**) Quantification of the type of experiments depicted in (A). Bars represent mean ± SEM ($n = 4$; $^{**}P < 0.005$). (**C**) Cells were transfected with various constructs as indicated, LRRK2 variants were affinity-purified using GTP-agarose beads, and input and GTP-bound protein subjected to western blot analysis using an anti-GFP antibody. (**D**) Quantification of the type of experiments depicted in (C). Bars represent mean ± SEM ($n = 4$; $^{**}P < 0.005$). (**E**) Cells were transfected with various constructs as indicated, and LRRK2 variants affinity-purified and subjected to western blot analysis as described above. (**F**) Quantification of the type of experiments depicted in (E). Bars represent mean ± SEM ($n = 5$; $^{*}P < 0.05$; $^{**}P < 0.005$). (**G**) Cells were transfected with the various constructs as indicated, and LRRK2 variants affinity-purified and subjected to western blot analysis followed by quantification as described above. Bars represent mean ± SEM ($n = 4$; $^{*}P < 0.05$; $^{**}P < 0.01$).

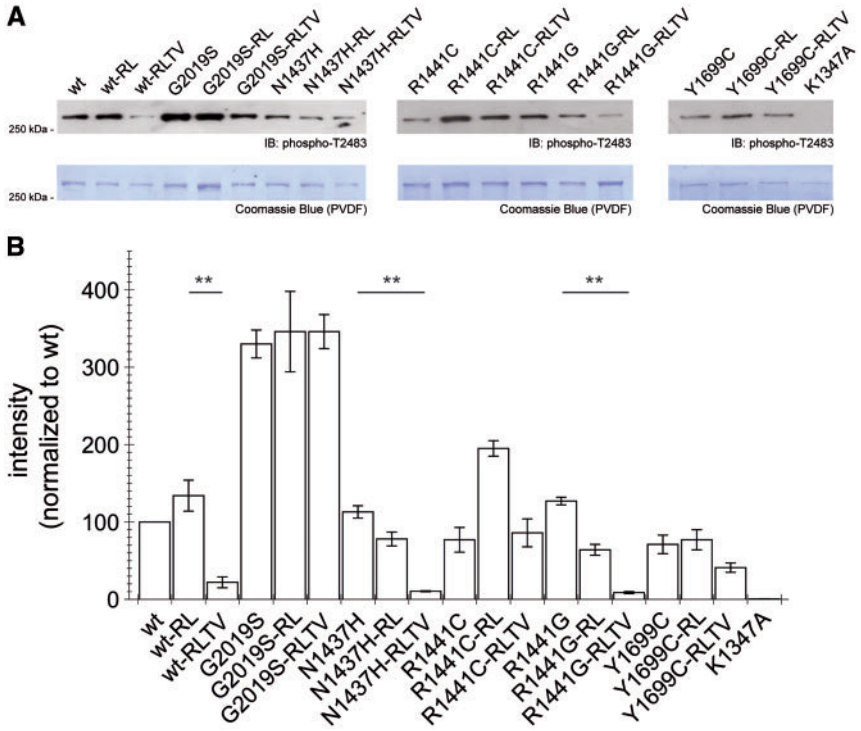

Figure 11. Effects of RL and RLTV mutations on LRRK2 kinase activity. (A) Example of autophosphorylation of distinct LRRK2 proteins as indicated. Autophosphorylation was detected with an antibody against phospho-Thr2483 (top) and was normalized to protein input as measured by Coomassie Blue staining (bottom). (B) Quantification of the type of experiments as depicted in (A), with values normalized to autophosphorylation of wild-type LRRK2. Bars represent mean ± SEM ($n = 4$; $^{**}P < 0.001$).

that autophosphorylation at multiple distinct sites within LRRK2 may contribute toward modulating the enhanced localization of most pathogenic LRRK2 to MTs, but the generally low stoichiometry of such autophosphorylation events (61) makes this an unlikely possibility. Altogether, our data indicate that the altered subcellular localization of the various pathogenic LRRK2 mutants does not correlate with alterations in inherent LRRK2 kinase activity.

However, and in an apparently contradictory manner, various structurally distinct and specific LRRK2 kinase inhibitors all triggered the relocalization of wild-type and mutant LRRK2 to MTs, whilst such relocalization was not observed with two distinct kinase-dead point mutants (K1906M and T2035A). LRRK2 is phosphorylated by a variety of upstream cellular kinases at distinct sites within the N-terminus, including S910, S935, S955 and S973, and phosphorylation at these sites is important for 14-3-3 binding (36,61,66,67). Pharmacological kinase inhibition has been suggested to be associated with a conformational change associated with dephosphorylation of the N-terminal phosphorylation sites, and such dephosphorylation was not found with two distinct synthetic kinase-dead mutants, suggesting that these mutants may not properly mimick the features of pharmacologically kinase-inhibited LRRK2 (50). We corroborated these findings, and further found that dephosphorylation of the N-terminal phosphorylation sites was observed in the presence of pharmacological kinase inhibitor in the case of the T2035A, but not the K1906M mutant. Thus, and in contrast to the T2035A mutant, the K1906M mutant may not be able to bind kinase inhibitor and/or may not be able to undergo an inhibitor-mediated conformational change. The differential dephosphorylation of the N-terminal sites correlated with the differential ability of those mutants to form a filamentous phenotype in the presence of pharmacological kinase inhibition, indicating that N-terminal dephosphorylation parallels the altered subcellular localization of pharmacologically kinase-inhibited LRRK2.

Apart from pharmacologically kinase-inhibited LRRK2, all pathogenic mutants which displayed enhanced filament formation are known to show decreased N-terminal phosphorylation and 14-3-3 binding (36,61,66,67). Increasing cellular 14-3-3 levels reverted the filamentous phenotype of both pathogenic and kinase-inhibited LRRK2, which correlated with increased N-terminal phosphorylation and decreased GTP binding. To determine whether dephosphorylation of the N-terminus of LRRK2 is sufficient to cause a filamentous phenotype, we mutated all currently known N-terminal phosphorylation sites implicated in 14-3-3 binding. As previously described, Ala mutations of S910 and S935, but not of S955 or S973 were without effect on the filamentous phenotype, but caused a relocalization of LRRK2 into the dot-like phenotype. Mutating two distinct residues (S910 and S1444) also implicated in 14-3-3 binding (71) caused a similar subcellular relocalization. Whilst the identity of those dot-like structures remains unclear, the observation that a pharmacological kinase inhibitor was able to relocalize those mutant proteins back into a filamentous phenotype suggests that these structures are not irreversible protein aggregates. Our data suggest that N-terminal dephosphorylation is not sufficient to cause the filamentous phenotype of pathogenic or pharmacologically kinase-inhibited LRRK2. In addition, no significant changes in N-terminal phosphorylation were observed when altering the GTP-binding status of LRRK2 by either mutational or pharmacological means, even though such

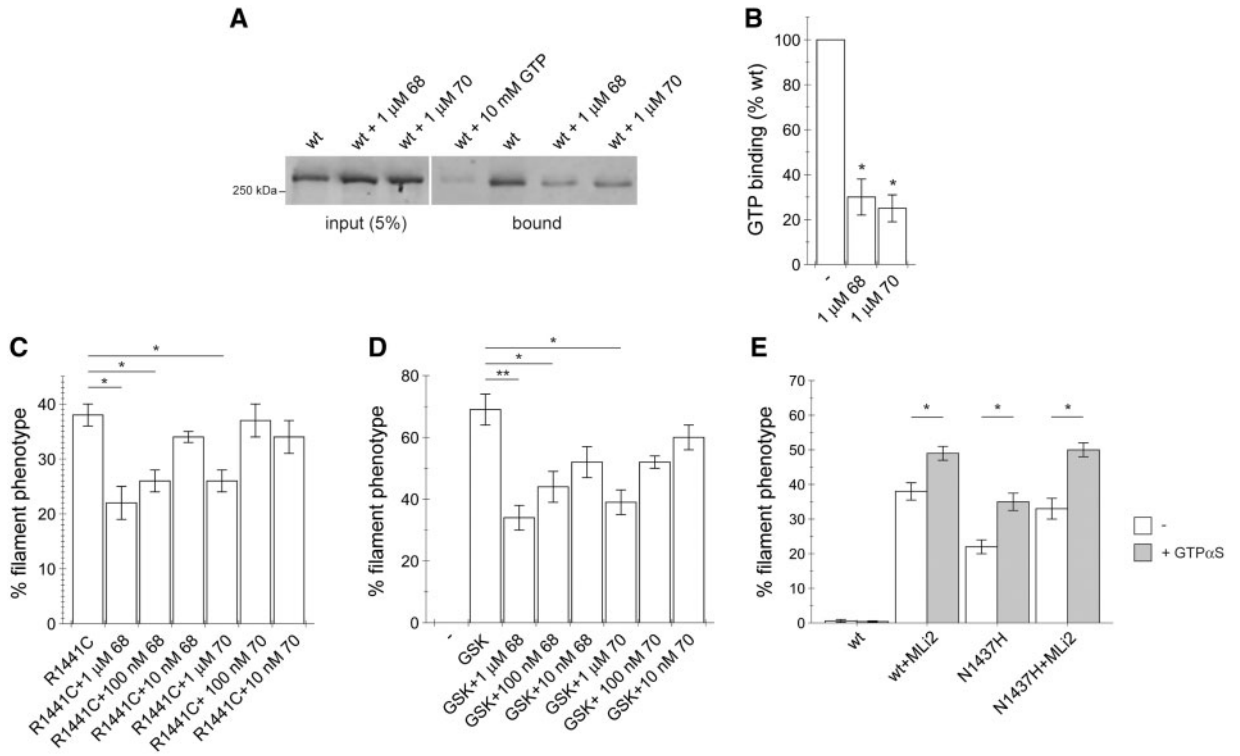

Figure 12. LRRK2 GTP-binding inhibitors decrease, and GTP analogs increase the filamentous phenotype. (**A**) Example of GTP binding of wild-type LRRK2 in the absence or presence of two distinct GTP-binding inhibitors as indicated. Inhibitors were added during cell lysis, and were present throughout binding. Input (5%) and GTP-bound proteins were subjected to western blot analysis using an anti-GFP antibody. (**B**) Quantification of the type of experiments depicted in (A). Bars represent mean ± SEM ($n = 3$; *$P < 0.005$). (**C**) Cells were transfected with R1441C-pathogenic LRRK2, and treated for 3 h with the respective concentration of GTP-binding inhibitors as indicated prior to analysis for LRRK2 subcellular localization. Bars represent mean ± SEM ($n = 3$; *$P < 0.05$). (**D**) Cells were transfected with wild-type LRRK2, treated for 1 h with GTP-binding inhibitors as indicated, followed by addition of 1 μM GSK2578215A and incubation for another 2 h before fixation and analysis for LRRK2 subcellular localization. Bars represent mean ± SEM ($n = 3$; **$P < 0.01$; *$P < 0.05$). (**E**) Cells were transfected as indicated and treated with 500 nM MLi2 for 2 h before permeabilization as indicated. Cells were permeabilized with streptolysin-O for 10 min, and incubated in resealing buffer for another 10 min both in the presence or absence of GTPαS or 500 nM MLi2 as indicated, followed by fixation and analysis for LRRK2 subcellular localization. Bars represent mean ± SEM ($n = 3$; *$P < 0.05$).

manipulations profoundly affected the subcellular localization of LRRK2. Therefore, N-terminal dephosphorylation also does not seem to be necessary for the observed changes in subcellular localization.

To further understand the shared mechanism underlying the filamentous phenotype of both pathogenic mutant and pharmacologically kinase-inhibited LRRK2, we probed for possible effects related to GTP binding. The GTP domain has been shown to exhibit important roles for the biological functions of LRRK2 (16,23–26,40,41,72,73), even though the precise mechanism(s) of action remain unclear. We observed a perfect correlation between increased steady-state levels of GTP binding of mutant as well as of pharmacologically kinase-inhibited LRRK2 with the enhanced colocalization with MTs, indicating that increased steady-state GTP binding may explain the convergence onto a common cellular readout. We next used both molecular as well as pharmacological approaches to determine whether interfering with LRRK2 GTP binding would revert the altered subcellular localization. Residues R1398 and T1343 have been implicated in GTP binding according to structural and biochemical studies (23,37), and careful biochemical analysis has shown that mutating these residues has no impact on protein stability and/or macromolecular structure (26). In agreement with the importance of those residues for LRRK2 function (26), mutations of RL or RLTV caused a drastic decrease in steady-state levels of GTP binding of all pathogenic LRRK2 mutants, which was paralleled by a decrease in the filamentous phenotype in the absence as well as presence of kinase inhibitors. Interestingly, the RH substitution reported to confer protection against PD (6–9) also decreased the filamentous phenotype of mutant or pharmacologically kinase-inhibited LRRK2, which was associated with a decrease in steady-state GTP binding. Whilst the precise mechanism by which this variant protects against PD risk remains to be further elucidated, it is tempting to speculate that GTP-binding-mediated alterations in the subcellular localization may play a contributing role.

Previous studies reported either increased (RL) or decreased (RLTV) GTP hydrolysis activity of wild-type and G2019S-mutant LRRK2, with no changes observed in GTP binding (26). Such opposing effects on GTP hydrolysis do not parallel the observed decrease in filament formation with both mutants as found here. In addition, a recent study also reported a decrease in steady-state GTP binding of the protective RH variant when compared with wild-type LRRK2 (78). Whilst the lack of altered GTP binding of RL and RLTV mutants as reported previously (26) remains unclear, it may be due to subtle assay differences combined with the inherently low GTP binding affinity of LRRK2 *per se*. In either case, the reported decrease in GTP binding of the protective RH variant (78), together with our current data highlight the importance of the R1398 residue for steady-state GTP binding.

As proof-of-concept, we analyzed the effects of two recently identified small-molecule LRRK2 GTP-binding inhibitors (40,41). Both compounds interfered with steady-state GTP binding *in*

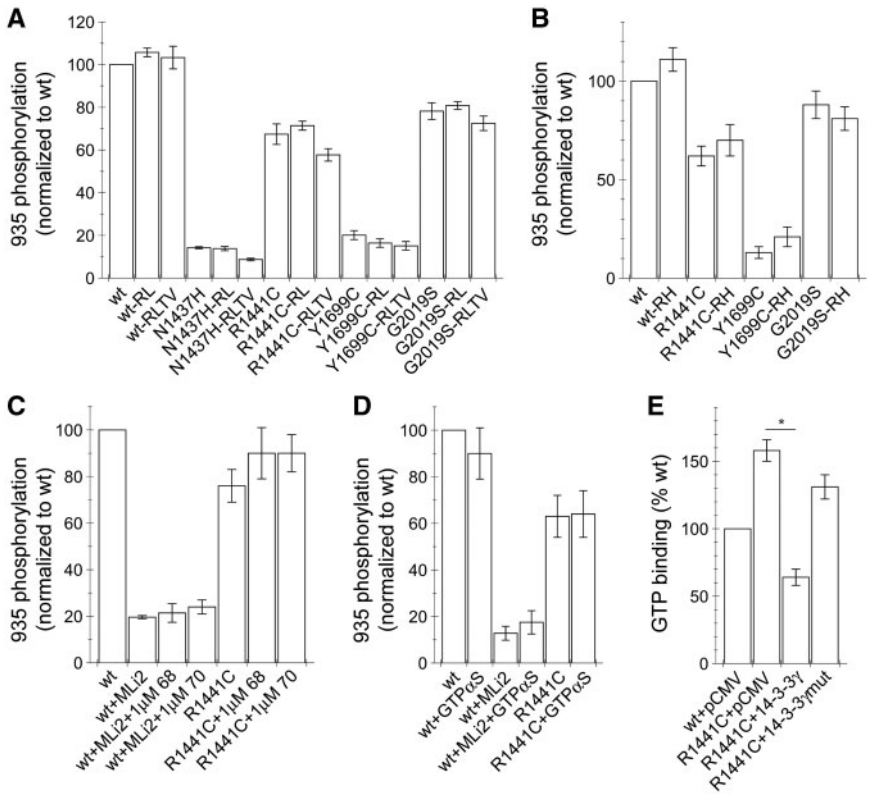

Figure 13. Alterations in the N-terminal phosphorylation status of LRRK2 are not necessary to cause a filamentous phenotype. (**A**) Cells were transfected with the indicated constructs, extracts analyzed for phosphorylated (S935) or total LRRK2 as indicated, and phospho-S935 signals normalized to wild-type LRRK2. Bars represent mean ± SEM ($n = 4$). (**B**) Cells were transfected with the indicated constructs, and extracts analyzed as described in (A). Bars represent mean ± SEM ($n = 5$). (**C**) Cells were transfected with the indicated constructs, treated with 500 nM MLi2 and/or with 1 μM GTP-binding inhibitors as indicated, and extracts analyzed for phospho-S935 signals as described in (A). Bars represent mean ± SEM ($n = 5$). (**D**) Cells were transfected with the indicated constructs, treated with 500 nM MLi2 for 2 h before permeabilization in the absence or presence of GTPαS as indicated, and analysis of extracts performed as described in (A). Bars represent mean ± SEM ($n = 5$). (**E**) Cells were transfected with the indicated constructs, LRRK2 variants were affinity-purified using GTP-agarose beads, and GTP-bound protein subjected to analysis for phospho-S935 signals as described in A. Bars represent mean ± SEM ($n = 3$; *$P < 0.05$).

vitro, and significantly reduced the enhanced colocalization of mutant or pharmacologically kinase-inhibited LRRK2 with MTs. These GTP-binding inhibitors have also been reported to reduce LRRK2 kinase activity in serum-starved cells (40). However, since all pharmacological LRRK2 kinase inhibitors analyzed here were found to increase the filamentous phenotype, the main mechanism of action of the GTP inhibitor compounds is most likely related to interfering with LRRK2 GTP binding rather than with kinase activity. Whilst promising lead compounds, they are unlikely to be highly specific for LRRK2-mediated GTP binding, but may modulate GTP binding of many other proteins. Thus, future studies in intact animal models using synthetic mutations which interfere with GTP binding (e.g. the protective RH risk variant) will be required to determine whether modulating GTP binding can abolish the detrimental effects of pathogenic LRRK2, as this would warrant further efforts to develop specific GTP-binding inhibitors to treat LRRK2-related PD due to ROC–COR mutations.

To obtain direct evidence that GTP binding is required for filament formation, we transiently permeabilized cells in the presence or absence of a non-hydrolyzable GTP analog. Addition of a non-hydrolyzable GTP analog did not induce filament formation of wild-type LRRK2, which may be due to differences in the conformational state of both pathogenic and pharmacologically kinase-inhibited LRRK2 versus wild-type LRRK2, in conjunction with the low inherent GTP binding affinity of wild-type LRRK2. However, addition of a non-hydrolyzable GTP analog increased the filamentous phenotype of both pathogenic and kinase-inhibited LRRK2, providing formal proof that GTP binding is crucial for the altered subcellular localization of pathogenic and pharmacologically kinase-inhibited LRRK2.

Amongst all pathogenic LRRK2 mutants, only the G2019S mutation has been consistently shown to display increased kinase activity when measured *in vitro* (80,81), whilst not displaying increased GTP binding or association with MTs when compared with wild-type. In contrast, all ROC–COR mutants showed unaltered kinase activity *in vitro*, but increased GTP binding and a filamentous phenotype. Conversely, both G2019S and filament-forming LRRK2 mutants were found to cause increased phosphorylation of certain Rab proteins when measured from intact cells (81). Rab proteins are associated with distinct vesicular structures moving along MT tracks. Therefore, the enhanced MT association of ROC–COR mutants may cause increased substrate phosphorylation due to enhanced 'molecular proximity', without an inherent increase in kinase activity. Whilst further studies will be necessary to corroborate the detailed downstream effects of the pathogenic LRRK2-mediated MT interactions, our results suggest a model whereby the distinct pathogenic LRRK2 mutants may impact upon the same intracellular MT-mediated vesicular trafficking events, albeit doing so by distinct means.

Materials and Methods

Reagents

Trichostatin A, tubacin and nocodazole were from Sigma Aldrich, PTL from Eurodiagnostico, LRRK2-IN1, TAE684 and CZC25146 from the Michael J. Fox Foundation, GSK2578215A from Tocris, compound 68 (ID 9108605) and compound 70 (ID 9119202) from Chembridge Corporation (San Diego, USA), and GNE-0877 and GNE-7915 from MedchemExpress (USA), and MLi2 from MRC PPU, Dundee, UK. Natural streptolysin-O was from Abcam (ab63978), and non-hydrolyzable GTP test kit from Jena Bioscience (NK-102).

DNA constructs and site-directed mutagenesis

GFP-tagged human wild-type, R1441C, Y1699C, G2019S and K1347A LRRK2 constructs were obtained from Addgene. All other constructs were generated by site-directed mutagenesis (QuickChange, Stratagene), and the identity of constructs verified by sequencing of the entire coding region. For transfection purposes, DNA was prepared from bacterial cultures grown at 37 °C using a midiprep kit (Promega) according to the manufacturer's instructions. GFP-tagged human α-tubulin K40 acetyltransferase (αTAT1) and an enzymatically inactive point mutant (D157N) (62) were from Addgene. Both wild-type and mutant αTAT1 were PCR amplified and subcloned into pDsRED-Express vector using the *Ba*MHI and *Eco*RI sites to generate C-terminally tagged dsRED-constructs. Human flag-tagged ARHGEF7 and the GEF-dead variant (L386R/L387S) were generous gifts from Drs K. Haebig and M. Bonin (University of Tuebingen, Germany), human V5-tagged ArfGAP1 was a generous gift from Dr T. Dawson (Johns Hopkins University, Baltimore, USA), human HA-tagged RGS2 was a generous gift from Dr. B. Wolozin (Boston University School of Medicine, Boston, USA), and human flag-HA-tagged 14-3-3β and rat flag-HA-tagged 14-3-3γ were from Addgene. The binding-deficient V181D mutant 14-3-3γ construct was generated by site-directed mutagenesis, and identity of the construct verified by sequencing of the coding region.

Cell culture and transfections

HEK293T/17 cells were cultured as previously described (90) and transfected at 80% confluence with 2 μg of LRRK2 constructs and 6 μl of LipoD293 (SignaGen Laboratories) per well of a six-well plate overnight in full medium. Cotransfections were performed with 1.8 μg of LRRK2 constructs and 200 ng of constructs as indicated (400 ng for 14-3-3 constructs). Cells were split onto coverslips the following day at a ratio of 1:4. As indicated, cells were incubated with nocodazole (200 nM), trichostatin A (800 nM), tubacin (10 μM), LRRK2-IN1 (1 μM), TAE684 (200 nM), CZC25146 (200 nM), GSK2578215A (1 μM), GNE-0877 (1 μM), GNE-7915 (1 μM), compound 68 (10 nM to 1 μM), compound 70 (10 nM to 1 μM) for 3 h in full medium, or with PTL (5 or 10 μM) for 12 h in full medium, followed by fixation and processing for immunochemistry, or by cell lysis and western blot analysis as described in following sections.

Immunofluorescence and laser confocal imaging

MT staining was performed essentially as described (91). Briefly, cells were rinsed twice in PBS, followed by fixation in 3% formaldehyde, 0.2% glutaraldehyde, 0.2% Triton X-100, 10 mM EGTA for 10 min at 37 °C. Fixed cells were washed two times in PBS for 5 min each, followed by quenching with 50 mM ammonium chloride in PBS for 10 min at RT, and two washes in PBS for 5 min each. Fixed cells were permeabilized in 0.1% Triton X-100 in PBS for 10 min, washed in PBS, blocked in 1% BSA (w/v) in PBS for 20 min, and incubated with primary antibodies in PBS for 1 h. Primary antibodies included mouse monoclonal anti-α-tubulin (Sigma Aldrich, clone DM1A, 1:100), mouse monoclonal anti-β-tubulin (Millipore, clone KMX-1, 1:100), mouse monoclonal anti-acetylated α-tubulin (Sigma, clone 6-11B-1, 1:100), rabbit polyclonal anti-detyrosinated α-tubulin (Abcam, ab48389, 1:200; or Millipore, AB3201, 1:500), rat monoclonal anti-tyrosinated α-tubulin (Abcam, ab6160, 1:100), or rat monoclonal anti-HA (Roche, clone 3F10, 1:500).

Secondary antibodies included Alexa 647-conjugated goat anti-rabbit, goat anti-mouse or goat anti-rat, or Alexa 488-conjugated goat anti-mouse, goat anti-rabbit or goat anti-rat antibodies (Invitrogen, 1:1000). Coverslips were incubated with secondary antibodies for 1 h at RT, followed by washes in PBS and mounting using mounting medium containing DAPI (Vector Laboratories).

Images were acquired on a Leica TCS-SP5 confocal microscope using a 63× 1.4 NA oil UV objective (HCX PLAPO CS). Images were collected using single excitation for each wavelength separately and dependent on secondary antibodies (488 nm Argon Laser line and a 510–540 nm emission band pass; 633 HeNe Laser line and a 640–670 nm emission band pass). GFP-tagged proteins were excited with 488 nm Argon Laser line and a 500–530 nm emission band pass, and DAPI was excited with the 405 nm UV diode and a 430–480 nm emission band pass, respectively.

Twenty-five image sections of selected areas were acquired with a step size of 0.3 μm, and z-stack images analyzed and processed using Leica Applied Systems (LAS AF6000) image acquisition software. For deconvolution, image sections of selected areas were acquired with a step size of 0.12 μm, and deconvolved using Huygens Essential Deconvolution software.

Quantification of colocalization of mutant or kinase-inhibited LRRK2 with acetylated or detyrosinated α-tubulin was performed essentially as described (82). For each condition, five individual cells were analyzed. Eight LRRK2-positive MT tracks were randomly selected from each cell and a line drawn over the length of a straight part of the track. Tracks were scored for the level of colocalization using image calculator and plot profile functions of ImageJ. The percentage of colocalization was subgrouped for each cell, with colocalization 0–50% (white), 50–90% (gray) or >90% (dark gray).

For the determination of the subcellular localization of GFP-tagged LRRK2 proteins, cells were transfected and cultured as described, and fixed 48 h after transfection in 4% paraformaldehyde in PBS for 20 min at RT. Fixed cells were washed two times in PBS, permeabilized in 0.5% Triton X-100 in PBS for 10 min at RT, washed in PBS, and mounted in mounting medium containing DAPI (Vector Laboratories). Cells were visualized on an inverted microscope (Zeiss) using a 100× 1.40 NA Plan APO oil objective. For each experiment, 100 random cells were scored and assigned to one of three phenotypes [cytosolic: purely diffuse localization; dot-like: presence of at least one dot-like structure (small, usually perinuclear); filamentous: presence of clear filamentous structures]. Experiments with RL, TV and RLTV mutants, and experiments involving LRRK2 GTP-binding inhibitors were performed and analyzed by two independent observers blind to condition, with comparable results obtained in all cases.

Live cell imaging

Live cell imaging of HEK293T/17 cells transfected with GFP-tagged wild-type LRRK2 was performed on cells grown on glass-bottom dishes (IBIDI) in full medium without phenol red. Live images were acquired 48 h after transfection on a Leica TCS-SP5 confocal microscope using a 63× 1.4 NA oil UV objective (HCX PLAPO CS). LRRK2-IN1 (1 μM final concentration) was added at time 0, and images collected using single excitation 488 nm Argon Laser line and a 495–575 nm emission band pass. The 488 nm Argon Laser line was set at 30%, with pinhole airy at 1. Contrast phase images of single stacks were simultaneously acquired. Fifteen image sections of selected areas were acquired every 45 s with a step size of 0.5 μm. Z-stack maximal intensity projection images were analyzed and processed using Leica Applied Systems (LAS AF6000) image acquisition software.

MT nucleation assays

Cells were grown and transfected as described above, and split onto poly-L-lysine-coated coverslips 24 h later. The following day, coverslips in six-well dishes were placed in an ice-water bath for 1.5 h to cause cold-induced MT depolymerization. MT regrowth was initiated by placing coverslips at 37 °C for the indicated time periods, followed by fixation in 4% paraformaldehyde in a buffer containing 60 mM PIPES, 25 mM HEPES, pH 6.9, 10 mM EGTA, 1 mM $MgCl_2$ and 0.5% Triton X-100 (92) before immunostaining as described above. Cells were visualized on an inverted microscope (Zeiss) using a 100× 1.40 NA Plan APO oil objective. For each timepoint, 100 cells were scored for visible MT staining with antibodies against α-tubulin or acetylated α-tubulin in non-transfected versus transfected cells, and for visible pathogenic LRRK2 filament reformation in transfected cells.

Permeabilization of cells with streptolysin-O

Cells were grown and transfected as described above, and split onto poly-L-lysine-coated coverslips in 24-well plates the following day. Two days after transfection, cells were incubated with or without 500 nM MLi2 for 2 h as indicated. Permeabilization was performed essentially as described previously (93,94) with slight modifications. Cells were permeabilized in 1 ml of Hank's balanced salt solution (HBSS; 4.17 mM $NaHCO_3$, 0.34 mM Na_2HPO_4, 0.44 mM KH_2PO_4, 137.9 mM NaCl, 5.3 mM KCl, pH 7.4) containing 16 ng/ml streptolysin-O for 10 min at 37 °C. This resulted in the permeabilization of around 80% of cells as independently determined by Trypan blue staining. After 10 min, permeabilization buffer was replaced by 1 ml of resealing buffer (10 mM HEPES, 140 mM NaCl, 5 mM KCl, 1.3 mM $MgCl_2$, 2 mM $CaCl_2$, pH 7.4), and cells were incubated for an additional 10 min at 37 °C. Buffers contained 500 nM MLi2, 5 μM GTPαS, GPCpp, GppCp, GppNHp or GTPγS as indicated. Amongst the non-hydrolyzable GTP analogs tested, only GTPαS was found to be non-toxic to permeabilized cells up to a concentration of 5 μM, and thus was used for all subsequent experiments. Upon permeabilization and resealing, cells were fixed and stained as described above, and 100 random cells were scored for a filamentous phenotype per condition and experiment. Cells displayed an intact MT network upon 10 min permeabilization and 10 min resealing under all conditions analyzed.

Cell extracts and western blotting

Cells were collected 48 h after transfection, washed in PBS and resuspended in cell lysis buffer (1% SDS in PBS containing 1 mM PMSF, 1 mM Na_3VO_4, 5 mM NaF). Extracts were sonicated, boiled and centrifuged at 13 500 rpm for 10 min at 4 °C. Protein concentration of supernatants was estimated using the BCA assay (Pierce), and equal amount of extracts were resolved by SDS-PAGE, transferred to PVDF (in the case of ECL detection) or to nitrocellulose membranes (in the case of detection by Odyssey) and analyzed by western blotting using a variety of antibodies as indicated, including rabbit polyclonal anti-GFP (Abcam, ab6556, 1:1000), mouse monoclonal anti-myc (Sigma, clone 9E10, 1:1000), rabbit polyclonal anti-V5 (Sigma, V8137, 1:2500), rat monoclonal anti-HA (Roche, clone 3F10, 1:500), mouse monoclonal anti-flag (Sigma, clone M2, 1:500), phospho-S935-LRRK2 antibody (Abcam, 1:1000), mouse monoclonal anti-acetylated α-tubulin (Sigma, clone 6-11B-1, 1:5000), rabbit polyclonal anti-detyrosinated α-tubulin (Millipore, AB3201, 1:500) and mouse monoclonal anti-α-tubulin (Sigma, clone DM1A, 1:10 000). Membranes were incubated with primary antibodies in 5% BSA (w/v) in TBS–0.1% Tween-20 for 1.5 h at RT, or overnight at 4 °C. For ECL detection, membranes were incubated with secondary antibodies in 5% BSA in TBS–0.1% Tween-20 for 1 h, or with secondary antibodies in PBS (1:10 000) for detection by Odyssey, followed by three times 5 min rinses in PBS. Westerns were developed with ECL reagents (Roche), and a series of timed exposures to ensure that densitometric analyses were performed at exposures within the linear range. Most determinations of steady-state protein levels, as well as all GTP-binding assays were quantified by ODYSSEY infrared imaging system application software LI-COR Image Studio Lite version 5.2.

For determination of S935-phosphorylation status, HEK293T cells were transiently transfected with the indicated constructs to express wild-type or mutant LRRK2 using 1 μg of DNA in 50 μl OPTI-MEM (Thermo Fisher) and 2 μg of linear polyethylenimine (PEI, Polyscience) per P24 well. Cells were lysed 48 h after transfection with 100 μl of lysis buffer [20 mM Tris–HCl, pH 7.5, 150 mM NaCl, 1 mM EDTA, 1% Triton, 10% glycerol, supplemented with Protease and Phosphatase Inhibitor Mixture (Roche)]. Samples were incubated on ice for 30 min and cleared by centrifugation at 18 000*g* for 30 min at 4 °C. Protein concentration of supernatants was estimated using the BCA assay (Pierce), and equal amount of protein (10 μg) were resolved on 3–8% SDS-PAGE, transferred onto PVDF membranes (Bio-Rad) and analyzed by immunofluorescence western blotting using antibodies against total-LRRK2 antibody (N241 A/34, NeuroNab, 1:1000) or anti-GFP antibody (Abcam, ab6556, 1:1000), phospho-S935-LRRK2 antibody [UDD2 10(12), Abcam, 1:1000] and mouse monoclonal anti-beta-actin (Sigma, 1:10 000). Membranes were incubated with primary antibodies in 5% BSA (w/v) in TBS–0.1% Tween-20 overnight at 4 °C. Membranes were washed three times for 10 min with TBS–Tween buffer, and incubated for 1.5 h at room temperature with anti-mouse Alexa-488 and anti-rabbit Alexa-568 secondary antibodies (1:1000) in 5% BSA (w/v) in TBS-T buffer. Membranes were washed in TBS-T buffer followed by visualization on Typhoon FLA9500 (GE Healthcare) and densitometry analysis carried out using ImageJ software. In some cases, analysis was performed as described above by ODYSSEY infrared imaging system application software LI-COR Image Studio Lite version 5.2. In all cases, total LRRK2 protein levels were comparable amongst the different mutants analyzed.

GTP-binding assays

GTP-binding assays were performed essentially as previously described (77). HEK293T/17 cells were cultured in 100 mm diameter dishes and transfected at 70–80% confluence with 12 μg of GFP-tagged LRRK2 DNA and 36 μl of LipoD293 per plate. Cells were split into 100 mm dishes at a ratio of 1:3 the following day, and lysed in 1 ml of lysis buffer per dish [20 mM Tris–HCl, pH 7.4, 1% Triton X-100, 137 mM NaCl, 3 mM KCl, 10% (v/v) glycerol, 1 mM EDTA, 1 mM Na_3VO_4, 5 mM NaF, 1 mM PMSF] for 1 h at 4 °C on a rotary wheel, followed by clarification of extracts by centrifugation at 13 200 rpm for 10 min at 4 °C. Soluble protein was evenly split into two tubes to a final volume of 500 μl each, and each incubated with 30 μl of 5'-GTP agarose beads (Sigma Aldrich) overnight at 4 °C on a rotary wheel. One of the two samples was used as control for non-specific binding to GTP-agarose beads by adding a final concentration of 10 mM GTP. The next day, beads were washed two times with ice-cold lysis buffer, and GTP-bound proteins eluted from beads by incubation with 30 μl ice-cold lysis buffer containing 10 mM GTP for 15 min at 4 °C on a rotary wheel. Beads were centrifuged at 13 200 rpm for 1 min, eluates were transferred to fresh tubes and resuspended with 5× Laemmli sample buffer containing β-mercaptoethanol. Both eluate and input (5% total lysate) samples were subjected to SDS-PAGE and western blotting with an anti-GFP antibody (Abcam, ab6556, 1:1000). GTP-binding assays were quantified by ODYSSEY as described above, with GTP-specific binding of each LRRK2 construct normalized to protein input. For experiments determining the effects of GTP-binding inhibitors (40,41), the respective compounds were added to the lysis buffer and kept throughout the experiment. For experiments determining the effect of LRRK2 kinase inhibitors, compounds were added to cells 4 h prior to lysis, added to the lysis buffer, and kept throughout the experiment.

In vitro LRRK2 kinase assays

pDEST53-GFP-LRRK2 wild-type and mutants were transiently transfected into HEK293T/17 cells using 20 μg of DNA in 1 ml OPTI-MEM (Thermo Fisher) and 40 μl of linear PEI (Polyscience) (20 μM) per 10 cm^2 Petri dish. Cells were harvested 48 h after transfection with 500 μl of lysis buffer [10 mM Tris–HCl, pH 7.5, 150 mM NaCl, 5 mM EDTA, 2.5 mM $Na_4P_2O_7$, 1 mM β-glycerophosphate, 1 mM Na_3VO_4, supplemented with Protease Inhibitor Mixture (Sigma Aldrich) and 1% (v/v) Tween-20]. Samples were incubated on ice for 30 min, and centrifuged at 18 000*g* for 35 min at 4 °C. Supernatants were incubated overnight with 20 μl of GFP-Trap beads (ChromoTek GmbH, Planegg, Germany) at 4 °C with mild agitation. Beads were sequentially washed with 500 μl of buffer 1 [20 mM Tris–HCl, pH 7.5, 500 mM NaCl, 1% (v/v) Tween-20], buffer 2 [20 mM Tris–HCl, pH 7.5, 350 mM NaCl, 1% (v/v) Tween-20], buffer 3 [20 mM Tris–HCl, pH 7.5, 150 mM NaCl, 1% (v/v) Tween-20], buffer 4 [20 mM Tris–HCl, pH 7.5, 150 mM NaCl, 0.1% (v/v) Tween-20] and buffer 5 [20 mM Tris–HCl, pH 7.5, 150 mM NaCl, 0.02% (v/v) Tween-20]. GFP-LRRK2-containing beads were resuspended in 100 μl of kinase buffer [25 mM Tris–HCl, pH 7.5, 5 mM β-glycerophosphate, 2 mM DTT, 0.1 mM Na_3VO_4, 10 mM $MgCl_2$ supplemented with 0.007% (v/v) Tween-20] for subsequent *in vitro* kinase assays.

Kinase reactions were started by addition of ATP (200 μM final) and were incubated for 1 h at 30 °C with mild agitation. Samples were centrifuged, supernatants discarded and proteins eluted from beads by addition of Laemmli sample buffer and boiling for 5 min at 95 °C. Samples (10 μl) were separated by SDS-PAGE, and transferred onto PVDF membranes (Bio-Rad) using the Trans-Blot Turbo Transfer System (Bio-Rad) in semi-dry conditions using 1× Trans-Blot Turbo Transfer Buffer (Bio-Rad) in 20% (v/v) ethanol at 25 V for 20 min. Membranes were blocked for 40 min in 5% (w/v) skimmed milk in TBS-T buffer [20 mM Tris–HCl, pH 7.4, 150 mM NaCl, 0.1% (v/v) Tween-20], followed by incubation for 1 h with an antibody against the LRRK2 autophosphorylation site T2483 (MJF-R8, Abcam, 1:2000). Membranes were washed four times for 10 min with TBS-T buffer, and incubated for 1 h at room temperature with horseradish peroxidase-conjugated rabbit secondary antibodies (1:15 000) in 5% (w/v) skimmed milk in TBS-T buffer. Membranes were washed in TBS-T buffer followed by visualization using ECL Western Blotting Detection Reagents (GE Healthcare). Data were normalized to the concentration of the individual proteins on PVDF membranes directly stained with Coomassie [40% methanol, 10% acetic acid, 0.1% (w/v) Comassie R-250], and densitometry analysis carried out using ImageJ software, with kinase activities of the various proteins expressed relative wild-type LRRK2, which was present on every gel for comparison.

Statistical analysis

All data are expressed as means ± SEM. Data were analyzed by one-way ANOVA with Tukey's post hoc test, and $P < 0.05$ was considered significant.

Acknowledgements

We thank Laura Montosa for excellent technical assistance with microscopy, and Drs T. Dawson, B. Wolozin, K. Haebig and M. Bonin for generously providing a variety of constructs used in the present study.

Conflict of Interest statement. None declared.

Funding

S.H. is supported by the Michael J. Fox Foundation, the BBVA Foundation, FEDER, and the Spanish Ministry of Economy and Competitiveness (SAF2014-58653-R). Funding to pay the Open Access publication charges for this article was provided by SAF2014-58653-R.

References

1. Lees, A.J., Hardy, J. and Revesz, T. (2009) Parkinson's disease. *Lancet*, **373**, 2055–2066.
2. Zimprich, A., Biskup, S., Leitner, P., Lichtner, P., Farrer, M., Lincoln, S., Kachergus, J., Hulihan, M., Uitti, R.J., Calne, D.B. *et al.* (2004) Mutations in LRRK2 cause autosomal-dominant Parkinsonism with pleomorphic pathology. *Neuron*, **44**, 601–607.
3. Paisán-Ruíz, C., Jain, S., Evans, E.W., Gilks, W.P., Simón, J., van der Brug, M., López de Munaín, A., Aparicio, S., Gil, A.M., Khan, N. *et al.* (2004) Cloning of the gene containing mutations that cause PARK8-linked Parkinson's disease. *Neuron*, **44**, 595–600.
4. Simón-Sánchez, J., Schulte, C., Bras, J.M., Sharma, M., Gibbs, J.R., Berg, D., Paisan-Ruiz, C., Lichtner, P., Scholz, S.W., Hernandez, D.G. *et al.* (2009) Genome-wide association study reveals genetic risk underlying Parkinson's disease. *Nat. Genet.*, **41**, 1308–1312.
5. Satake, W., Nakabayashi, Y., Mizuta, I., Hirota, Y., Ito, C., Kubo, M., Kawaguchi, T., Tsunoda, T., Watanabe, M., Takeda, A. *et al.* (2009) Genome-wide association study identifies

common variants at four loci as genetic risk factors for Parkinson's disease. *Nat. Genet.*, **41**, 1303–1307.
6. Tan, E.K., Peng, R., Teo, Y.Y., Tan, L.C., Angeles, D., Ho, P., Chen, M.L., Lin, C.H., Mao, X.Y., Chang, X.L. *et al.* (2010) Multiple LRRK2 variants modulate risk of Parkinson disease: a Chinese multicenter study. *Hum. Mutat.*, **31**, 561–568.
7. Ross, O.A., Soto-Ortolaza, A.I., Heckman, M.G., Aasly, J.O., Abahuni, N., Annesi, G., Bacon, J.A., Bardien, S., Bozi, M., Brice, A. *et al.* (2011) Association of LRRK2 exonic variants with susceptibility to Parkinson's disease: a case-control study. *Lancet Neurol.*, **10**, 898–908.
8. Chen, L., Zhang, S., Liu, Y., Hong, H., Wang, H., Zheng, Y., Zhou, H., Chen, J., Xian, W., He, Y. *et al.* (2011) LRRK2 R1398H polymorphism is associated with decreased risk of Parkinson's disease in a Han Chinese population. *Parkinsonism Relat. Disord.*, **17**, 291–292.
9. Heckman, M.G., Elbaz, A., Soto-Ortolaza, A.I., Serie, D.J., Aasly, J.O., Annesi, G., Augurger, G., Bacon, J.A., Boczarka-Jedynak, M., Bozi, M. *et al.* (2014) Protective effect of LRRK2 p.R1398H on risk of Parkinson's disease is independent of MAPT and SNCA variants. *Neurobiol. Aging*, **35**, 266.e5–214.
10. Mata, I.F., Wedemeyer, W.J., Farrer, M.J., Taylor, J.P. and Gallo, K.A. (2006) LRRK2 in Parkinson's disease: protein domains and functional insights. *Trends Neurosci.*, **29**, 286–293.
11. Cardona, F., Tormos-Pérez, M. and Pérez-Tur, J. (2014) Structural and functional *in silico* analysis of LRRK2 missense substitutions. *Mol. Biol. Rep.*, **41**, 2529–2542.
12. West, A.B., Moore, D.J., Biskup, S., Bugayenko, A., Smith, W.W., Ross, C.A., Dawson, V.L. and Dawson, T.M. (2005) Parkinson's disease-associated mutations in leucine-rich repeat kinase 2 augment kinase activity. *Proc. Natl. Acad. Sci. U.S.A.*, **102**, 16842–16847.
13. Greggio, E., Jain, S., Kingsbury, A., Bandopadhyay, R., Lewis, P., Kaganovich, A., van der Brug, M.P., Beilina, A., Blackinton, J., Thomas, K.J. *et al.* (2006) Kinase activity is required for the toxic effects of mutant LRRK2/dardarin. *Neurobiol. Dis.*, **23**, 329–341.
14. Jaleel, M., Nichols, R.J., Deak, M., Campbell, D.G., Gillardon, F., Knebel, A. and Alessi, D.R. (2007) LRRK2 phosphorylates moesin at threonine-558: characterization of how Parkinson's disease mutants affect kinase activity. *Biochem. J.*, **405**, 307–317.
15. Ito, G., Okai, T., Fujino, G., Takeda, K., Ichijo, H., Katada, T. and Iwatsubo, T. (2007) GTP binding is essential to the protein kinase activity of LRRK2, a causative gene product for familial Parkinson's disease. *Biochemistry*, **46**, 1380–1388.
16. West, A.B., Moore, D.J., Choi, C., Andrabi, S.A., Li, X., Dikeman, D., Biskup, S., Zhang, Z., Lim, K.L., Dawson, V.L. and Dawson, T.M. (2007) Parkinson's disease-associated mutations in LRRK2 link enhanced GTP-binding and kinase activities to neuronal toxicity. *Hum. Mol. Genet.*, **16**, 223–232.
17. Aasly, J.O., Vilariño-Guell, C., Dachsel, J.C., Webber, P.J., West, A.B., Haugarvoll, K., Johansen, K.K., Toft, M., Nutt, J.G., Payami, H. *et al.* (2010) Novel pathogenic LRRK2 p.Asn1437His substitution in familial Parkinson's disease. *Mov. Disord.*, **25**, 2156–2163.
18. Liao, J., Wu, C.W., Burlak, C., Zhang, S., Sahm, H., Wang, M., Zhang, Z.Y., Vogel, K.W., Federici, M., Riddle, S.M. *et al.* (2014) Parkinson disease-associated mutation R1441H in LRRK2 prolongs the "active state" of its GTPase domain. *Proc. Natl. Acad. Sci. U.S.A.*, **111**, 4055–4060.
19. Lewis, P.A., Greggio, E., Beilina, A., Jain, S., Baker, A. and Cookson, M.R. (2007) The R1441C mutation of LRRK2 disrupts GTP hydrolysis. *Biochem. Biophys. Res. Commun.*, **357**, 668–671.
20. Li, X., Tan, Y.C., Poulose, S., Olanow, C.W., Huang, X.Y. and Yue, Z. (2007) Leucine-rich repeat kinase 2 (LRRK2)/PARK8 possesses GTPase activity that is altered in familial Parkinson's disease R1441C/G mutants. *J. Neurochem.*, **103**, 238–247.
21. Cookson, M.R. (2015) LRRK2 pathways leading to neurodegeneration. *Curr. Neurol. Neurosci. Rep.*, **15**, 42.
22. Smith, W.W., Pei, Z., Jiang, H., Dawson, V.L., Dawson, T.M. and Ross, C.A. (2006) Kinase activity of mutant LRRK2 mediates neuronal toxicity. *Nat. Neurosci.*, **9**, 1231–1233.
23. Xiong, Y., Coombes, C.E., Kilaru, A., Li, X., Gitler, A.D., Bowers, W.J., Dawson, V.L., Dawson, T.M. and Moore, D.J. (2010) GTPase activity plays a key role in the pathobiology of LRRK2. *PLoS Genet*, **6**, e1000902.
24. Stafa, K., Trancikova, A., Webber, P.J., Glauser, L., West, A.B. and Moore, D.J. (2012) GTPase activity and neuronal toxicity of Parkinson's disease-associated LRRK2 is regulated by ArfGAP1. *PLoS Genet.*, **8**, e1002526.
25. Xiong, Y., Yuan, C., Chen, R., Dawson, T.M. and Dawson, T.L. (2012) ArfGAP1 is a GTPase activating protein for LRRK2: reciprocal regulation of ArfGAP1 by LRRK2. *J. Neurosci.*, **32**, 3877–3886.
26. Biosa, A., Trancikova, A., Civiero, L., Glauser, L., Bubacco, L., Greggio, E. and Moore, D.J. (2013) GTPase activity regulates kinase activity and cellular phenotypes of Parkinsons's disease-associated LRRK2. *Hum. Mol. Genet.*, **22**, 1140–1156.
27. Fuji, R.N., Flagella, M., Baca, M., Baptista, M.A., Brodbeck, J., Chan, B.K., Fiske, B.K., Honigberg, L., Jubb, A.M., Katavolos, P. *et al.* (2015) Effect of selective LRRK2 kinase inhibition in nonhuman primate lung. *Sci. Transl. Med.*, **7**, 273ra15.
28. Fell, M.J., Mirescu, C., Basu, K., Cheewatrakoolpong, B., DeMong, D.E., Ellis, J.M., Hyde, L.A., Lin, Y., Markgraf, C.G., Mei, H. *et al.* (2015) MLi-2, a potent, selective and centrally active compound for exploring the therapeutic potential and safety of LRRK2 kinase inhibition. *J. Pharmacol. Exp. Ther.*, **355**, 397–409.
29. Taymans, J.M. and Greggio, E. (2016) LRRK2 kinase inhibition as a therapeutic strategy for Parkinson's disease, where do we stand? *Curr. Neuropharmacol.*, **14**, 214–225.
30. Gómez-Suaga, P., Fdez, E., Fernández, B., Martínez-Salvador, M., Blanca Ramírez, M., Madero-Pérez, J., Rivero-Ríos, P., Fuentes, J.M. and Hilfiker, S. (2014) Novel insights into the neurobiology underlying LRRK2-linked Parkinson's disease. *Neuropharmacology*, **85**, 45–56.
31. Gandhi, P.N., Wang, X., Zhu, X., Chen, S.G. and Wilson-Delfosse, A.L. (2008) The Roc domain of leucine-rich repeat kinase 2 is sufficient for interaction with microtubules. *J. Neurosci. Res.*, **86**, 1711–1720.
32. Caesar, M., Zach, S., Carlson, C.B., Brockmann, K., Gasser, T. and Gillardon, F. (2013) Leucine-rich repeat kinase 2 functionally interacts with microtubules and kinase-dependently modulates cell migration. *Neurobiol. Dis.*, **54**, 280–288.
33. Gillardon, F. (2009) Leucine-rich repeat kinase 2 phosphorylates brain tubulin-beta isoforms and modulates microtubule stability-a point of convergence in Parkinsonian neurodegeneration? *J. Neurochem.*, **110**, 1514–1522.
34. Kett, L.R., Boassa, D., Ho, C.C., Rideout, H.J., Hu, J., Terada, M., Ellisman, M. and Dauer, W.T. (2012) LRRK2 Parkinson disease mutations enhance its microtubule association. *Hum. Mol. Genet.*, **21**, 890–899.
35. Godena, V.K., Brookes-Hocking, N., Moller, A., Shaw, G., Oswald, M., Sancho, R.M., Miller, C.C., Whitworth, A.J. and De Vos, K.J. (2014) Increasing microtubule acetylation

rescues axonal transport and locomotor deficits caused by LRRK2 ROC–COR domain mutations. *Nat. Commun.*, **5**, 5245.
36. Dzamko, N., Deak, M., Hentati, F., Reith, A.D., Prescott, A.R., Alessi, D.R. and Nichols, R.J. (2010) Inhibition of LRRK2 kinase activity leads to dephosphorylation of Ser(910)/Ser(935), disruption of 14-3-3 binding and altered cytoplasmic localization. *Biochem. J.*, **430**, 405–413.
37. Deng, X., Dzamko, N., Prescott, A., Davies, P., Liu, Q., Yang, Q., Lee, J.D., Patricelli, M.P., Nomanbhoy, T.K., Alessi, D.R. and Gray, N.S. (2011) Characterization of a selective inhibitor of the Parkinson's disease kinase LRRK2. *Nat. Chem. Biol.*, **7**, 203–205.
38. Sheng, Z., Zhang, S., Bustos, D., Kleinheinz, T., Le Pichon, C.E., Dominguez, S.L., Solanoy, H.O., Drummond, J., Zhang, X., Ding, X. *et al.* (2012) Ser1292 autophosphorylation is an indicator of LRRK2 kinase activity and contributes to the cellular effects of PD mutations. *Sci. Trans. Med.*, **4**, 164ra161.
39. Thomas, J.M., Li, T., Yang, W., Xue, F., Fishman, P.S. and Smith, W.W. (2017) 68 and FX2149 attenuate mutant LRRK2-R1441C-induced neural transport impairment. *Front. Aging Neurosci.*, **8**, 337.
40. Li, T., Yang, D., Zhong, S., Thomas, J.M., Xue, F., Liu, J., Kong, L., Voulalas, P., Hassan, H.E., Park, J.S. *et al.* (2014) Novel LRRK2 GTP-binding inhibitors reduced degeneration in Parkinson's disease cell and mouse models. *Hum. Mol. Genet.*, **23**, 6212–6222.
41. Li, T., He, X., Thomas, J.M., Yang, D., Zhong, S., Xue, F. and Smith, W.W. (2015) A novel GTP-binding inhibitor, FX2149, attenuates LRRK2 toxicity in Parkinson's disease models. *PLoS ONE*, **10**, e0122461.
42. Zhang, J., Deng, X., Choi, H.G., Alessi, D.R. and Gray, N.S. (2012) Characterization of TAE684 as a potent LRRK2 kinase inhibitor. *Bioorg. Med. Chem. Lett.*, **22**, 1864–1869.
43. Ramsden, N., Perrin, J., Ren, Z., Lee, B.D., Zinn, N., Dawson, V.L., Tam, D., Bova, M., Lang, M., Drewes, G. *et al.* (2011) Chemoproteomics-based design of potent LRRK2-selective lead compounds that attenuate Parkinson's disease-related toxicity in human neurons. *ACS Chem. Biol.*, **6**, 1021–1028.
44. Reith, A.D., Bamborough, P., Jandu, K., Andreotti, D., Mensah, L., Dossang, P., Choi, H.G., Deng, X., Zhang, J., Alessi, D.R. and Gray, N.S. (2012) GSK2578215A; A potent and highly selective 2-arylmethyloxy-5-substituent-N-arylbenzamide LRRK2 kinase inhibitor. *Bioorg. Med. Chem. Lett.*, **22**, 5625–5629.
45. Estrada, A.A., Liu, X., Baker-Glenn, C., Beresford, A., Burdick, D.J., Chambers, M., Chan, B.K., Chen, H., Ding, X., DiPasquale, A.G. *et al.* (2012) Discovery of highly potent, selective, and brain-penetrable leucine-rich repeat kinase 2 (LRRK2) small molecular inhibitors. *J. Med. Chem.*, **55**, 9416–9433.
46. Estrada, A.A., Chan, B.K., Baker-Glenn, C., Beresford, A., Burdick, D.J., Chambers, M., Chen, H., Dominguez, S.L., Dotson, J., Drummond, J. *et al.* (2014) Discovery of highly potent, selective, and brain-penetrant aminopyrazole leucine-rich repeat kinase 2 (LRRK2) small molecule inhibitors. *J. Med. Chem.*, **57**, 921–936.
47. Tomiyama, H., Li, Y., Funayama, M., Hasegawa, K., Yoshino, H., Kubo, S., Sato, K., Hattori, T., Lu, C.S., Inzelberg, R. *et al.* (2006) Clinicogenetic study of mutations in LRRK2 exon 41 in Parkinson's disease patients from 18 countries. *Mov. Disord.*, **21**, 1102–1108.
48. Funayama, M., Hasegawa, K., Ohta, E., Kawashima, N., Komiyama, M., Kowa, H., Tsuji, S. and Obata, F. (2005) An LRRK2 mutation as a cause for the parkinsonism in the original PARK8 family. *Ann. Neurol.*, **57**, 918–921.
49. Greggio, E., Zambrano, I., Kaganovich, A., Beilina, A., Taymans, J.M., Daniels, V., Lewis, P., Jain, S., Ding, J., Syed, A. *et al.* (2008) The Parkinson's disease-associated leucine-rich repeat kinase 2 (LRRK2) is a dimer that undergoes intramolecular autophosphorylation. *J. Biol. Chem.*, **283**, 16906–16914.
50. Ito, G., Fujimoto, T., Kamikawaji, S., Kuwahara, T. and Iwatsubo, T. (2014) Lack of correlation between the kinase activity of LRRK2 harboring kinase-modifying mutations and its phosphorylation at Ser910, 935, and Ser955. *PLoS ONE*, **9**, e97988.
51. Wloga, D. and Gaertig, J. (2010) Post-translational modifications of microtubules. *J. Cell Sci.*, **123**, 3447–3455.
52. Song, Y. and Brady, S.T. (2015) Post-translational modifications of tubulins: pathways to functional diversity of microtubules. *Trends Cell Biol.*, **25**, 125–136.
53. Janke, C. (2014) The tubulin code: molecular components, readout mechanisms, and functions. *J. Cell Biol.*, **206**, 461–472.
54. Peris, L., Wagenbach, M., Lafanechère, L., Brocard, J., Moore, A.T., Kozielski, F., Job, D., Wordeman, L. and Andrieux, A. (2009) Motor-dependent microtubule disassembly driven by tubulin tyrosination. *J. Cell Biol.*, **185**, 1159–1166.
55. Matsuyama, A., Shimazu, T., Sumida, Y., Saito, A., Yoshimatsu, Y., Seigneurin-Berny, D., Osada, H., Komatsu, Y., Nishino, N., Khochbin, S. *et al.* (2002) *In vivo* destabilization of dynamic microtubules by HDAC6-mediated deacetylation. *EMBO J.*, **21**, 6820–6831.
56. Haggarty, S.J., Koeller, K.M., Wong, J.C., Grozinger, C.M. and Schreiber, S.L. (2003) Domain-selective small-molecule inhibitor of histone deacetylase 6 (8HDAC6)-mediated tubulin deacetylation. *Proc. Natl. Acad. Sci. U.S.A.*, **100**, 4389–4394.
57. Shida, T., Cueva, J.G., Xu, Z., Goodman, M.B. and Nachury, M.V. (2010) The major a-tubulin K40 acetyltransferase aTAT1 promotes rapid ciliogenesis and efficient mechanosensation. *Proc. Natl. Acad. Sci. U.S.A.*, **107**, 21517–21522.
58. Kalebic, N., Martinez, C., Perlas, E., Hublitz, P., Bilbao-Cortes, D., Fiedorczuk, K., Andolfo, A. and Heppenstall, P.A. (2013) Tubulin acetyltransferase aTAT1 destabilizes microtubules independently of its acetylation activity. *Mol. Cell Biol.*, **33**, 1114–1123.
59. Fonrose, X., Ausseil, F., Soleilhac, E., Masson, V., David, B., Pouny, I., Cintrat, J.C., Rousseau, B., Barette, C., Massiot, G. and Lafanechère, L. (2007) Parthenolide inhibits tubulin carboxypeptidase activity. *Cancer Res.*, **67**, 3371–3378.
60. Barisic, M., Silva e Sousa, R., Tripathy, S.K., Magiera, M.M., Zaytsev, A.V., Pereira, A.L., Janke, C., Grishchuk, E.L. and Maiato, H. (2015) Mitosis. Microtubule detyrosination guides chromosomes during mitosis. *Science*, **348**, 799–803.
61. Gloeckner, C.J., Boldt, K., von Zweydorf, F., Helm, S., Wiesent, L., Sarioglu, H. and Ueffing, M. (2010) Phosphopeptide analysis reveals two discrete clusters of phosphorylation in the N-terminus and the Roc domain of the Parkinson-disease associated protein kinase LRRK2. *J. Proteome Res.*, **9**, 1738–1745.
62. Greggio, E., Taymans, J.M., Zhen, E.Y., Ryder, J., Vancraenenbroeck, R., Beilina, A., Sun, P., Deng, J., Jaffe, H., Baekelandt, V., Merchant, K. and Cookson, M.R. (2009) The Parkinson's disease kinase LRRK2 autophosphorylates its GTPase domain at multiple sites. *Biochem. Biophys. Res. Commun.*, **389**, 449–454.
63. Kamikawaji, S., Ito, G. and Iwatsubo, T. (2009) Identification of the autophosphorylation sites of LRRK2. *Biochemistry*, **48**, 10963–10975.

64. Pungaliya, P.P., Bai, Y., Lipinski, K., Anand, V.S., Sen, S., Brown, E.L., Bates, B., Reinhart, P.H., West, A.B., Hirst, W.D. and Braithwaite, S.P. (2010) Identification and characterization of a leucine-rich repeat kinase 2 (LRRK2) consensus phosphorylation motif. *PLoS ONE*, **5**, e13672.
65. Webber, P.J., Smith, A.D., Sen, S., Renfrow, M.B., Mobley, J.A. and West, A.B. (2011) Autophosphorylation in the leucine-rich repeat kinase 2 (LRRK2) GTPase domain modifies kinase and GTP-binding activities. *J. Mol. Biol.*, **412**, 94–110.
66. Nichols, R.J., Dzamko, N., Morrice, N.A., Campbell, D.G., Deak, M., Ordureau, A., Macartney, T., Tong, Y., Shen, J., Prescott, A.R. and Alessi, D.R. (2010) 14-3-3 binding to LRRK2 is disrupted by multiple Parkinson's disease-associated mutations and regulates cytoplasmic localization. *Biochem. J.*, **430**, 393–404.
67. Doggett, E.A., Zhao, J., Mork, C.N., Hu, D. and Nichols, R.J. (2012) Phosphorylation of LRRK2 serines 955 and 973 is disrupted by Parkinson's disease mutations and LRRK2 pharmacological inhibition. *J. Neurochem.*, **120**, 37–45.
68. Lavalley, N.J., Slone, S.R., Ding, H., West, A.B. and Yacoubian, A.T. (2016) 14-3-3 proteins regulate mutant LRRK2 kinase activity and neurite shortening. *Hum. Mol. Genet.*, **25**, 109–122.
69. Li, X., Wang, Q.J., Pan, N., Lee, S., Zhao, Y., Chait, B.T. and Yue, X. (2011) Phosphorylation-dependent 14-3-3 binding to LRRK2 is impaired by common mutations of familial Parkinson's disease. *PLoS One*, **6**, e17153.
70. Darling, D.L., Yingling, J. and Wynshaw-Boris, A. (2005) Role of 14-3-3 proteins in eukaryotic signaling and development. *Curr. Top. Dev. Biol.*, **68**, 281–315.
71. Muda, K., Bertinetti, D., Besellchen, F., Hermann, J.S., von Zweydorf, F., Geerlof, A., Jacob, A., Ueffing, M., Gloeckner, C.F. and Herberg, F.W. (2014) Parkinson-related LRRK2 mutation R1441C/G/H impairs PKA phosphorylation of LRRK2 and disrupts its interaction with 14-3-3. *Proc. Natl. Acad. Sci. U.S.A.*, **111**, E34–E43.
72. Xiong, Y., Dawson, V.L. and Dawson, T.M. (2012) LRRK2 GTPase dysfunction in the pathogenesis of Parkinson's disease. *Biochem. Soc. Trans.*, **40**, 1074–1079.
73. Tsika, E. and Moore, D.J. (2013) Contribution of GTPase activity to LRRK2-associated Parkinson disease. *Small GTPases*, **4**, 164–170.
74. Dusonchet, J., Li, H., Guillily, M., Liu, M., Stafa, K., Derada Troletti, C., Boon, J.Y., Saha, S., Glauser, L., Mamais, A. *et al.* (2014) A Parkinson's disease gene regulatory network identifies the signaling protein RGS2 as a modulator of LRRK2 activity and neuronal toxicity. *Hum. Mol. Genet.*, **23**, 4887–4905.
75. Haebig, K., Gloeckner, C.J., Miralles, M.G., Gillardon, F., Schulte, C., Riess, O., Ueffing, M., Biskup, S. and Bonin, B. (2010) ARHGEF7 (BETA-PIX) acts as guanine nucleotide exchange factor for leucine-rich repeat kinase 2. *PLoS One*, **5**, e13762.
76. Deng, J., Lewis, P.A., Greggio, E., Sluch, E., Beilina, A. and Cookson, M.R. (2008) Structure of the ROC domain from the Parkinson's disease-associated leucine-rich repeat kinase 2 reveals a dimeric GTPase. *Proc. Natl. Acad. Sci. U.S.A.*, **105**, 1499–1504.
77. Chia, R., Haddock, S., Beilina, A., Rudenko, I.N., Mamais, A., Kaganovich, A., Li, Y., Kumaran, R., Nalls, M.A. and Cookson, M.R. (2014) Phosphorylation of LRRK2 by casein kinase 1a regulates trans-Golgi clustering via differential interaction with ARHGEF7. *Nat. Commun.*, **5**, 5827.
78. Nixon-Abell, J., Berwick, D.C., Grannó, S., Spain, V.A., Blackstone, C. and Harvey, K. (2016) Protective LRRK2 R1398H variant enhances GTPase and Wnt signaling activity. *Front. Mol. Neurosci.*, **8**, 9:18.
79. Taymans, J.M., Vancraenenbroeck, R., Ollikainen, P., Beilina, A., Lobbestael, E., De Maeyer, M., Baekelandt, V. and Cookson, M.R. (2011) LRRK2 kinase activity is dependent on LRRK2 GTP binding capacity but independent of LRRK2 GTP binding. *PLoS ONE*, **6**, e23207.
80. Greggio, E. and Cookson, M.R. (2009) Leucine-rich repeat kinase 2 mutations and Parkinson's disease: three questions. *ASN Neuro*, **1**, e00002.
81. Steger, M., Tonelli, F., Ito, G., Davies, P., Trost, M., Vetter, M., Wachter, S., Lorentzen, E., Duddy, G., Wilson, S. *et al.* (2016) Phosphoproteomics reveals that Parkinson's disease kinase LRRK2 regulates a subset of Rab GTPases. *Elife*, **5**, e12813.
82. Dunn, S., Morrison, E.E., Liverpool, T.B., Molina-París, C., Cross, R.A., Alonso, M.C. and Peckham, M. (2008) Differential trafficking of Kif5c on tyrosinated and detyrosinated microtubules in live cells. *J. Cell Sci.*, **121**, 1085–1095.
83. Jacobson, C., Schnapp, B. and Banker, G.A. (2006) A change in the selective translocation of the kinesin-1 motor domain marks the initial specification of the axon. *Neuron*, **49**, 797–804.
84. Konishi, Y. and Setou, M. (2009) Tubulin tyrosination navigates the kinesin-1 motor domain to axons. *Nat. Neurosci.*, **12**, 559–567.
85. Kaul, N., Soppina, V. and Verhey, K.J. (2014) Effects of a-tubulin K40 acetylation and detyrosination on kinesin-1 motility in a purified system. *Biophys. J.*, **106**, 2636–2643.
86. Cambray-Deakin, M.A. and Burgoyne, R.D. (1987) Posttranslational modifications of a-tubulin: acetylated and detyrosinated forms in axons of rat cerebellum. *J. Cell Biol.*, **104**, 1569–1574.
87. Sakaguchi-Nakashima, A., Meir, J.Y., Jin, Y., Matsumoto, K. and Hisamoto, N. (2007) LRK-1, a *C. elegans* PARK8-related kinase, regulates axonal-dendritic polarity of SV proteins. *Curr. Biol.*, **17**, 592–598.
88. Cirnaru, M.D., Marte, A., Belluzzi, E., Russo, I., Gabrielli, M., Longo, F., Arcuri, L., Murru, L., Bubacco, L., Matteoli, M. *et al.* (2014) LRRK2 kinase activity regulates synaptic vesicle trafficking and neurotransmitter release through modulation of LRRK2 macro-molecular complex. *Front. Mol. Neurosci.*, **7**, 49.
89. Goldstein, A.Y., Wang, X. and Schwarz, T.L. (2008) Axonal transport and the delivery of pre-synaptic components. *Curr. Opin. Neurobiol.*, **18**, 495–503.
90. Gómez-Suaga, P., Rivero-Ríos, P., Fdez, E., Blanca Ramírez, M., Ferrer, I., Aiastui, A., López de Munain, A. and Hilfiker, S. (2014) LRRK2 delays degradative receptor trafficking by impeding late endosomal budding through decreasing Rab7 activity. *Hum. Mol. Genet.*, **23**, 6779–6796.
91. Ciani, L. and Salinas, P.C. (2007) c-Jun N-terminal kinase (JNK) cooperates with Gsk3beta to regulate Dishevelled-mediated microtubule stability. *BMC Cell Biol.*, **8**, 27.
92. Choi, Y.K., Liu, P., Sze, S.K., Dai, C. and Qi, R.Z. (2010) CDK5RAP2 stimulates microtubule nucleation by the gamma-tubulin ring complex. *J. Cell Biol.*, **191**, 1089–1095.
93. Walev, I., Bhakdi, S.C., Hofmann, F., Djonder, N., Valeva, A., Aktories, K. and Bhakdi, S. (2001) Delivery of proteins into living cells by reversible membrane permeabilization with streptolysin-O. *Proc. Natl. Acad. Sci. U.S.A.*, **98**, 3185–3190.
94. Kano, F., Nakatsu, D., Noguchi, Y., Yamamoto, A. and Murata, M. (2012) A resealed-cell system for analyzing pathogenic intracellular events: perturbation of endocytic pathways under diabetic conditions. *PLoS ONE*, **7**, e44127.